Mon. Not. R. Astron. Soc. **000**, 1 (2004) Printed 5 February 2008 (MN LATEX style file v2.2)

Antonov Problem and Quasi-Equilibrium States in N-body System

Atsushi Taruya[1], Masa-aki Sakagami[2]
[1] *Research Center for the Early Universe(RESCEU), School of Science, University of Tokyo, Tokyo 113-0033, Japan*
[2] *Graduate School of Human and Environmental Studies, Kyoto University, Kyoto 606-8501, Japan*

5 February 2008

ABSTRACT
In this paper, a quantitative characterization for the evolutionary sequence of stellar self-gravitating system is investigated, focusing on the pre-collapse stage of the long-term dynamical evolution. In particular, we consider the quasi-equilibrium behaviors of the N-body systems in the setup of the so-called Antonov problem, i.e., self-gravitating N-body system confined in an adiabatic wall and try to seek a possible connection with thermostatistics of self-gravitating systems. For this purpose, a series of long-term N-body simulations with various initial conditions are performed. We found that a quasi-equilibrium sequence away from the thermal equilibrium can be characterized by the one-parameter family of the stellar models. Especially, the stellar polytropic distribution satisfying the effective equation of state $P \propto \rho^{1+1/n}$ provides an excellent approximation to the evolutionary sequence of the N-body system. Based on the numerical results, we discuss a link between the quasi-equilibrium state and the generalized thermostatistics by means of the non-extensive entropy.

Key words: stellar dynamics – methods: numerical – celestial mechanics – globular clusters: general

1 INTRODUCTION

1.1 Self-gravitating N-body systems and thermostatistics

The long-term dynamical evolution of stellar self-gravitating system driven by the two-body relaxation is an old problem with rich history in astronomy and astrophysics and even in statistical physics. The problem, in nature, involves the long-range attractive nature of gravity and because of its complexity and peculiarity as well as the physical reality, astronomers and statistical physicists have attracted much attention on this subject.

Historically, an important consequence from the thermodynamical arguments had arisen in the 1960s. Antonov (1962) first pointed out that no stable equilibrium state exists for a high-dense clusters. To prove this, he considered a very idealized situation called *Antonov problem*, i.e., a stellar self-gravitating system confined in a spherical cavity with radius r_e (see Fig.1). Then, under keeping the energy E and the mass M fixed, the standard statistical mechanical approach based on the maximum entropy principle leads to the conclusion that no stable equilibrium state exists for the larger radius $r_e > \lambda_{\rm crit}\,(-E/GM^2)$, where $\lambda_{\rm crit}$ is the critical value (Padmanabhan 1989, 1990, for pedagogical reviews). Note that the numerical value of $\lambda_{\rm crit}$ depends on the choice of the entropy and Antonov obtained $\lambda_{\rm crit} = 0.335$ in the case adopting the Boltzmann-Gibbs entropy:

$$S_{\rm BG} = -\int d^3\boldsymbol{x} d^3\boldsymbol{v}\ f(\boldsymbol{x},\boldsymbol{v})\ \ln\ f(\boldsymbol{x},\boldsymbol{v}), \tag{1}$$

where $f(\boldsymbol{x},\boldsymbol{v})$ is the one-particle distribution function in phase-space. Later, Lynden-Bell & Wood (1968) re-examined this issue and showed that the unstable thermal state found by Antonov can be explained by the thermodynamic instability arising from the negative specific heat. They especially called the instability *gravothermal catastrophe*.

Since the 1960s, the gravothermal instability discovered by Antonov has become a standard notion of the stellar dynamics and the role of the instability has been extensively discussed. Thanks to the unprecedented development of the computer facility as well as the sophisticated numerical techniques based on the N-body simulation and the Fokker-Planck calculation, our view of the late-time phase of the stellar gravitating system has dramatically improved (e.g., Meylan & Heggie 1997; Heggie & Hut 2003). Among various theoretical developments, one important landmark would be a discovery of the *gravothermal oscillation*, which was originally suggested by Sugimoto & Bettwieser (1983) (see also Bettwieser & Sugimoto 1984) and was later confirmed by numerical simulation (Makino 1996). With a great advantage of a special purpose hardware, GRAPE

(e.g., Sugimoto et al. 1990; Hut & Makino 1999), the core-collapse triggered by gravothermal instability was shown to be terminated by the formation of binary as a result of three-body interaction and the oscillatory behaviors of the core motion has been clearly revealed. The gravothermal oscillation is thus thought to be one of the most fundamental stellar dynamical processes and provides a basis to understand the dynamical history of globular clusters as real astronomical system.

So far the theory of long-term evolution in stellar self-gravitating systems has been developed without any recourse to the statistical mechanics or thermodynamics except for the seminal works by Antonov (1962) and Lynden-Bell & Wood (1968). This is essentially because the issues under consideration are, in nature, non-equilibrium problem with long-range interaction and usual sense of the thermal equilibrium becomes inadequate. Indeed, as Antonov (1962) emphasized, no strict meaning of the thermal equilibrium exists in the case of an isolated stellar system without boundary. Nevertheless, thermostatistical point-of-view is helpful in predicting the fate of the unstable system. This would be even true in the non-equilibrium situation as long as the collisional evolution during the relaxation timescales is concerned. In this sense, there might be some possibilities to recast the non-equilibrium self-gravitating systems in terms of an extended view of the thermostatistics. The present paper attempts to address these issues by considering an old problem of stellar dynamics from a somewhat new point-of-view. Especially, we wish to focus on the thermostatistical characterization of non-equilibrium self-gravitating system by means of the new thermostatistical formalism and discuss the validity of it.

Indeed, the self-gravitating system may be the best testing ground for the recent postulated introduction of a non-extensive generalization of Boltzmann-Gibbs statistics, originally proposed by Tsallis (1988). In contrast to the Boltzmann-Gibbs entropy (1) which is properly an extensive variable, the entropy used in the 'Tsallis' formalism is pseudo-additive and/or non-extensive one [1] :

$$S_q = -\frac{1}{q-1}\int d^3\boldsymbol{x}d^3\boldsymbol{v}\ \left[\{p(\boldsymbol{x},\boldsymbol{v})\}^q - p(\boldsymbol{x},\boldsymbol{v})\right], \tag{2}$$

where the probability $p(\boldsymbol{x},\boldsymbol{v})$ is not one-particle distribution function but a sort of primitive phase-space distribution that satisfies the normalization condition:

$$\int d^3\boldsymbol{x}d^3\boldsymbol{v}\ p(\boldsymbol{x},\boldsymbol{v}) = 1. \tag{3}$$

Note that the Boltzmann-Gibbs entropy (1) is recovered in the limit $q \to 1$ and in this limit, the primitive distribution is identified with the one-particle distribution.

Because of its non-extensive nature, the non-extensive 'Tsallis' formalism might have a potential to deal with the long-range systems including the self-gravitating systems. Further, it is expected to deal with a variety of interesting non-equilibrium problems such as quasi-steady state or quasi-equilibrium state far from the thermal equilibrium, to which the standard Boltzmann-Gibbs statistics cannot be applied (Tsallis 1999; Abe & Okamoto 2001, for comprehensive reviews). Nevertheless, most of the works on this subject are concerned with construction of a consistent formal framework and little works have been known concerning the physical realization of the non-extensive statistics. Hence, it seems interesting to address the issues on the reality of non-extensive statistics.

1.2 Non-extensive generalization of the thermostatistical description of self-gravitating system

Among various issues on the physical reality of the non-extensive thermostatistics, we have recently re-examined the classic problem considered by Antonov (1962) by means of the non-extensive thermostatistics with Tsallis' generalized entropy (Taruya & Sakagami 2002, 2003a,b,c; Sakagami & Taruya 2004, for a review). According to the framework using normalized q-expectation values by Tsallis, Mendes & Plastino (1998), the one-particle distribution $f(\boldsymbol{x},\boldsymbol{v})$ is expressed in terms of the primitive distribution $p(\boldsymbol{x},\boldsymbol{v})$ by (For the cases using standard linear-mean values, see Plastino & Plastino 1993; Taruya & Sakagami 2002):

$$f(\boldsymbol{x},\boldsymbol{v}) = M\frac{\{p(\boldsymbol{x},\boldsymbol{v})\}^q}{\displaystyle\int d^3\boldsymbol{x}d^3\boldsymbol{v}\ \{p(\boldsymbol{x},\boldsymbol{v})\}^q}. \tag{4}$$

Then, the standard analysis of statistical mechanics based on the Tsallis entropy (2) reveals that the extremum state of the entropy is reduced to the power-law distribution (Taruya & Sakagami 2003b):

$$f(\boldsymbol{x},\boldsymbol{v}) = A\left[\Phi_0 - \frac{1}{2}v^2 - \Phi(x)\right]^{q/(1-q)}, \tag{5}$$

where A and Φ_0 are the numerical constants and $\Phi(x)$ is the gravitational potential. In terms of the specific energy of a particle defined by $\epsilon = v^2/2 + \Phi(\boldsymbol{x})$, this gives $f \propto (\Phi_0 - \epsilon)^{q/(1-q)}$. Equation (5) is the famous one-parameter family of the stellar models referred to as the *stellar polytropic distribution* (e.g., Binney & Tremaine 1987) and the q-parameter is related to the polytrope index given by (Taruya & Sakagami 2003b):

[1] Strictly speaking, equation (2) is not exactly the same entropy as originally introduced by Tsallis in a sense that the entropy (2) is defined in μ-space, not in Γ-space. Nevertheless, we keep to call it Tsallis entropy because the thermostatistical framework with (2) that is constructed self-consistently is quite similar to the standard Tsallis formalism (see Taruya & Sakagami 2003b).

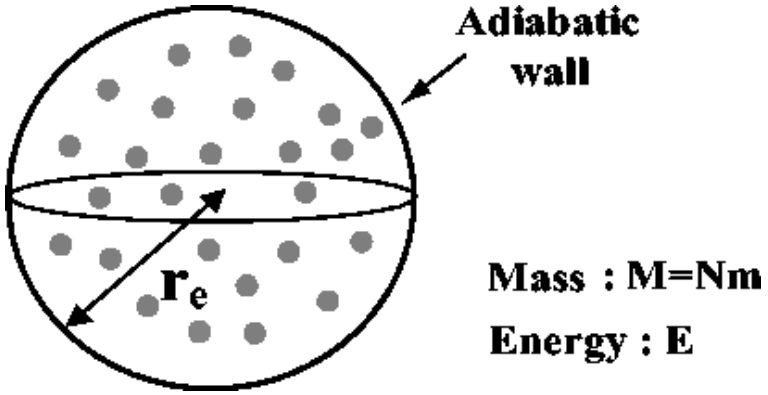

Figure 1. Setup of the Antonov problem.

$$n = \frac{1}{2} + \frac{1}{1-q}. \tag{6}$$

Similar to the case of the Boltzmann-Gibbs entropy (1), the statistical mechanical analysis based on the non-extensive entropy (2) also showed that there exists the thermodynamic instability, which can be consistently explained from the presence of the negative specific heat in terms of the non-extensive thermodynamics. Thus, the stellar polytropes as extremum states of Tsallis entropy are consistently characterized by the non-extensive thermostatistics and may play a role of the thermal equilibrium and/or quasi-equilibrium like the extremum state of the Boltzmann-Gibbs entropy. Nevertheless, concerning their reality, it is still unclear whether the consistent thermostatistical results really imply the existence of quasi-equilibrium state or not. In order to get a further insight into this issue, apart from the thermostatistical analysis, dynamical and/or kinematical aspects of the self-gravitating system should be investigated in details using the N-body simulation, which we will discuss here. Some of the work we report in this paper has already appeared in Letter form (Taruya & Sakagami 2003c). This paper further addresses new additional N-body experiments and an improved analysis, together with some careful discussions.

1.3 Outline of this paper

In section 2, within a setup of the classic issue considered by Antonov (1962) and Lynden-Bell & Wood (1968), we first address some important properties of the quasi-equilibrium distribution characterized by non-extensive entropy by comparing with those of the standard Boltzmann-Gibbs statistics. We then move to discuss the N-body simulations. In section 3, the N-body treatment of the Antonov problem is considered and the initial conditions are summarized. Section 4 is a main part of this paper, which describes the results of N-body experiments in details. After checking the N-body code in section 4.1, we discuss the quasi-equilibrium behaviors of the long-term evolution starting with the stellar polytropic distribution in section 4.2 and try to fit their evolutionary sequences by the stellar polytropes, which are shown to be a remarkably good fit. The results are also compared with an alternative one-parameter family of stellar model, i.e., the King model. In section 4.3, we attempt to clarify the condition for quasi-equilibrium state characterized by the stellar polytropes in other class of initial conditions, i.e., the stellar models with cusped density profile. Finally, section 5 is devoted to the discussion and the conclusion.

2 ANTONOV PROBLEM AND ITS NON-EXTENSIVE GENERALIZATION

In this section, we briefly mention the Antonov problem and the basic properties of the equilibrium states characterized by the extensive and the non-extensive entropies.

First recall the setup of the so-called Antonov problem. In this problem, we consider the many-body particle system confined in an adiabatic wall (see Fig.1). The radius of the wall is given by r_e and we assume that the total mass M and the total energy E are kept fixed. All the particles in this system interact via Newton gravity and bounce elastically from the wall. For further simplification, each particle is assumed to have the same mass m. Under these conditions, we consider a fully relaxed system and clarify the nature of stability or instability for such a system. Note that there are two characteristic time-scales in self-gravitating system. One is the dynamical time $t_{\rm dyn}$ and the other is the relaxation time $t_{\rm relax}$. Usually, for a system containing a large number of particles $N \gg 1$, these time-scales scale as $t_{\rm relax} \simeq (0.1N/\ln N)\, t_{\rm dyn}$ (e.g., Binney & Tremaine 1987). Accordingly, the equilibrium states considered here should be a long-lived state much longer than $t_{\rm relax}$ and thus the thermostatistical consideration becomes helpful.

In a language of thermostatistics, a fully relaxed equilibrium state corresponds to the state that maximizes the entropy. If we adopt the standard Boltzmann-Gibbs entropy (2), the equilibrium distribution is obtained by extremizing the entropy

$S_{\rm BG}$ under keeping the mass M and the energy E fixed:

$$M = \int d^3\boldsymbol{x} d^3\boldsymbol{v}\ f(\boldsymbol{x},\boldsymbol{v}), \tag{7}$$

$$E = \int d^3\boldsymbol{x} d^3\boldsymbol{v}\ \left[\frac{1}{2}\,v^2 + \frac{1}{2}\,\Phi(\boldsymbol{x})\right] f(\boldsymbol{x},\boldsymbol{v})\ \ ;\ \ \Phi(\boldsymbol{x}) = -G\int d^3\boldsymbol{x}' d^3\boldsymbol{v}'\ \frac{f(\boldsymbol{x}',\boldsymbol{v}')}{|\boldsymbol{x}-\boldsymbol{x}'|}. \tag{8}$$

Then the first variation of entropy with respect to f, i.e., $\delta[S_{\rm BG} - \alpha\ M - \beta\, E] = 0$ with α and β being Lagrange multipliers yields (Antonov 1962; Lynden-Bell & Wood 1968; Padmanabhan 1989):

$$f(\boldsymbol{x},\boldsymbol{v}) = \left(\frac{\beta}{2\pi}\right)^{3/2}\ \rho(\boldsymbol{x})\ e^{-\beta\, v^2/2} \tag{9}$$

with ρ being the mass density of the system defined by

$$\rho(\boldsymbol{x}) \equiv \int d^3\boldsymbol{v}\ f(\boldsymbol{x},\boldsymbol{v}). \tag{10}$$

Computing the pressure, one can deduce that equation of state is indeed isothermal in the case of the isotropic velocity distribution:

$$P(\boldsymbol{x}) \equiv \int d^3\boldsymbol{v}\ \frac{1}{3}v^2 f(\boldsymbol{x},\boldsymbol{v}), \tag{11}$$

which leads to $P(\boldsymbol{x}) = \beta^{-1}\rho(\boldsymbol{x})$.

On the other hand, if one uses the non-extensive entropy (2), the variational problem with respect to the primitive distribution $p(\boldsymbol{x},\boldsymbol{v})$ not the one-particle distribution $f(\boldsymbol{x},\boldsymbol{v})$ finally leads to the stellar polytropic distribution (5). With a help of the relation (6), this distribution can be rewritten with

$$f(\boldsymbol{x},\boldsymbol{v}) = \frac{1}{4\sqrt{2}\pi\ B(3/2, n-1/2)}\ \frac{\rho(\boldsymbol{x})}{\{(n+1)\,P(\boldsymbol{x})/\rho(\boldsymbol{x})\}^{3/2}}\ \left\{1 - \frac{v^2/2}{(n+1)\,P(\boldsymbol{x})/\rho(\boldsymbol{x})}\right\}^{n-3/2}, \tag{12}$$

where the function $B(a,b)$ represents the beta function. Note that we used the following relations to derive the above expression:

$$\rho(r) = 4\sqrt{2}\pi\, B\left(\frac{3}{2}, \frac{1}{1-q}\right)\ A\ [\Phi_0 - \Phi(r)]^{1/(1-q)+1/2}, \tag{13}$$

$$P(r) = \frac{8\sqrt{2}\pi}{3}\, B\left(\frac{5}{2}, \frac{1}{1-q}\right)\ A\ [\Phi_0 - \Phi(r)]^{1/(1-q)+3/2} \tag{14}$$

with r being the radius $r = |\boldsymbol{x}|$. These two equations lead to the polytropic equation of state:

$$P(r) = K_n \rho^{1+1/n}(r). \tag{15}$$

The explicit form of the dimensional constant K_n is given in Taruya & Sakagami (2003b) (Eq.(21) of their paper).

Comparing the distribution function (12) with (9), the stellar polytropic distribution can be reduced to the isothermal distribution when taking the limit $n \to +\infty$, and only in this limit, the isothermal equation of state is recovered. Basically, the equilibrium properties of the stellar polytropes are similar to those of the isothermal distribution. But, focusing on their thermodynamical stabilities, there exists some distinctive features. Before showing this, we first note that the one-particle distribution function (12) does not yet completely specify the equilibrium configuration, because functional forms of the density and the pressure are not determined. To determine the equilibrium configuration, we need to specify both $\rho(r)$ and $P(r)$, or equivalently the gravitational potential $\Phi(r)$. This can be achieved by solving the Poisson equation explicitly. Under the spherically symmetric configuration, the Poisson equation becomes

$$\frac{1}{r^2}\frac{d}{dr}\left\{r^2\frac{d\Phi(r)}{dr}\right\} = 4\pi G\rho(r). \tag{16}$$

or the condition of hydrostatic equilibrium:

$$\frac{dP(r)}{dr} = -\frac{Gm(r)}{r^2}\,\rho(r), \quad \frac{dm(r)}{dr} = 4\pi\rho(r)\,r^2, \tag{17}$$

where the quantity $m(r)$ denotes the mass inside the radius r. Denoting the central density and pressure by ρ_c and P_c, we then introduce the dimensionless quantities:

$$\rho = \rho_c\ [\theta(\xi)]^n\,, \quad r = \left\{\frac{(n+1)P_c}{4\pi G\rho_c^2}\right\}^{1/2}\ \xi, \tag{18}$$

which yields the following ordinary differential equation:

$$\theta'' + \frac{2}{\xi}\theta' + \theta^n = 0, \tag{19}$$

where prime denotes the derivative with respect to ξ. To obtain the physically relevant solution of (19), we put the following boundary condition:

$$\theta(0) = 1, \quad \theta'(0) = 0. \tag{20}$$

A family of solutions satisfying (20) is the *Emden solution*, which is well-known in the subject of stellar structure (e.g., see chapter IV of Chandrasekhar 1939). To characterize the equilibrium properties of Emden solutions, it is convenient to introduce the following set of variables, referred to as homology invariant variables (e.g., Chandrasekhar 1939; Kippenhahn & Wigert 1990):

$$u \equiv \frac{d\ln m(r)}{d\ln r} = \frac{4\pi r^3\rho(r)}{m(r)} = -\frac{\xi\theta^n}{\theta'}, \tag{21}$$

$$v \equiv -\frac{d\ln P(r)}{d\ln r} = \frac{\rho(r)}{P(r)}\,\frac{Gm(r)}{r} = -(n+1)\frac{\xi\theta'}{\theta}, \tag{22}$$

which reduce the degree of equation (19) from two to one. One can evaluate the total energy of the confined stellar system in terms of the pressure P_e ,the density ρ_e at the boundary r_e and the total mass M:

$$\begin{aligned} E &= \frac{3}{2}\int_0^{r_e} dr\, 4\pi r^2\, P(r) - \int_0^{r_e} dt\, \frac{Gm(r)}{r}\,\frac{dm}{dr} \\ &= -\frac{1}{n-5}\left[\frac{3}{2}\left\{\frac{GM^2}{r_e} - (n+1)\frac{MP_e}{\rho_e}\right\} + (n-2)\,4\pi\, r_e^3\, P_e\right], \end{aligned}$$

by which the dimensionless quantity λ can be expressed as a function of the homology invariant variables at the wall (Taruya & Sakagami 2002, 2003a,b):

$$\lambda \equiv -\frac{Er_e}{GM^2} = -\frac{1}{n-5}\left[\frac{3}{2}\left\{1 - \frac{n+1}{v_e}\right\} + (n-2)\frac{u_e}{v_e}\right]. \tag{23}$$

In figure 2 the dimensionless quantity λ is plotted as a function of the density contrast $D = \rho_c/\rho_e$, i.e., the ratio of the central density to that at the boundary. Each curves in (λ, D)-plane corresponds to the equilibrium sequence of stellar polytrope with a different value of polytrope index. For comparison, we also plot the equilibrium sequence of isothermal distribution in thick solid line. Figure 2 shows that the equilibrium sequences can be classified as two types. One is the the equilibrium sequences with indices $n \leqslant 5$. In this case, the λ-curves monotonically increase with density contrast. On the other hand, the other type of equilibrium sequences with $n > 5$ have peaks in each trajectory. At a certain value of the density contrast $D_{\rm crit}$, the trajectory reaches a maximum $\lambda_{\rm crit}$ and beyond this, the monotonicity is lost. This is even true in the limit $n \to +\infty$ and the maximum value of λ and the critical value of D can be read off (Antonov 1962; Lynden-Bell & Wood 1968; Padmanabhan 1989):

$$\lambda_{\rm crit} = 0.335, \quad D_{\rm crit} = 709. \tag{24}$$

In the case of Boltzmann-Gibbs entropy, it had been already known that, along the curve $\lambda(D)$ derived from the condition $\delta S_{\rm BG} = 0$, all states with $D > D_{\rm crit}$ are unstable. This can be proved by the turning-point analysis for a linear series of equilibria (Lynden-Bell & Wood 1968; Padmanabhan 1989; Katz 1978, 1979). Also, the same results can be obtained by explicitly evaluating the eigenmodes for the second variation of the entropy $\delta^2 S_{\rm BG}$ (Padmanabhan 1990, 1989). The absence of stable thermal equilibria in this regime clearly indicates the instability, referred to as the *the gravothermal catastrophe*.

In similar manner to the isothermal distribution, it has been recently shown that the stellar polytrope confined in an adiabatic wall exhibits the gravothermal instability in the case of the polytropic index $n > 5$. The evaluation of eigenvalues for the second variation of the Tsallis entropy $\delta^2 S_q$ also derives the same results as the above turning-point analysis in terms of the λ-curve (Taruya & Sakagami 2002, 2003a,b). Note that the gravothermal instability in the isothermal case is heuristically explained by the presence of negative specific heat. That is, the co-existence of the regions with negative and positive specific heat leads to the violation of thermal balance and finally causes the catastrophe temperature growth. This can be achieved when the radius of the adiabatic wall or equivalently the density contrast becomes sufficiently larger so that the effect of self-gravity is important at the inner dense region and becomes negligible at the outer sparse region. Although this intuitive explanation heavily relies on the standard notion of extensive thermostatistics, it is emphasized that the same interpretation can be possible in the case of the stellar polytropic distributions (Taruya & Sakagami 2003a). Therefore, despite some distinctive features, the stellar polytropes are consistently characterized as equilibrium distribution by means of the non-extensive formalism and their thermodynamic properties are similar to those of isothermal distribution.

Finally, the above arguments indicate that the stellar polytropic distribution might be regarded as a sort of thermal equilibrium, since it is the extrema of the Tsallis entropy. However, polytropic equation of state for the stellar polytropes clearly shows that the one-dimensional velocity dispersion defined by

$$\sigma^2_{\rm v,1D}(r) = \frac{P(r)}{\rho(r)} \tag{25}$$

manifestly depends on the radius r (see Eq.[15]). Only in the isothermal case $n \to \infty$, $\sigma_{\rm v,1D}$ is kept spatially constant. Thus, it is expected that a gradient of the velocity dispersion is relaxed on timescales of two-body encounter. This means that the

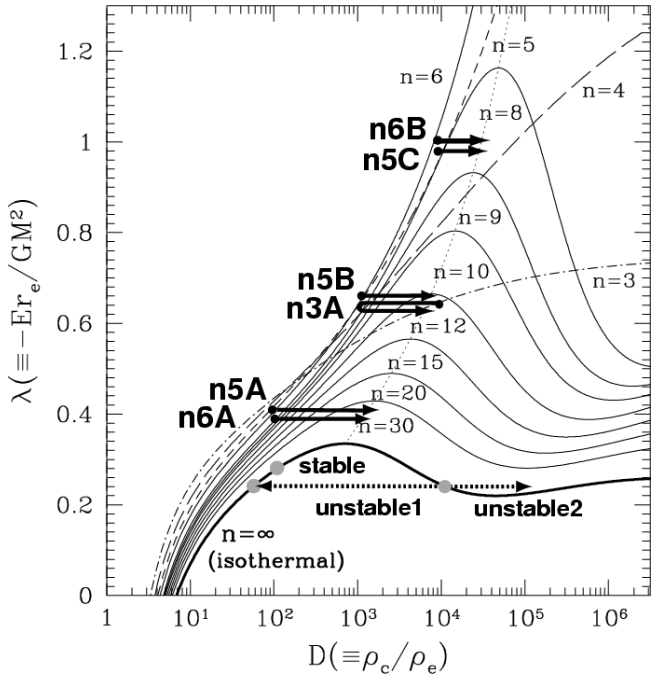

Figure 2. Energy-density contrast relationship of stellar polytropes and evolutionary tracks of the quasi-equilibrium states observed in the N-body experiments. Each curve represents equilibrium sequence of stellar polytrope with a different polytrope index n. The thin dotted line which traces the turning points for each equilibrium sequence is the marginal stability boundary inferred from the Tsallis entropy S_q. The thick arrows show the evolutionary tracks of N-body simulation starting with stellar polytropic and/or isothermal distributions (see table 1 and 2).

stellar polytrope is no longer the equilibrium but quasi-equilibrium state. At present, it might be also possible to give another interpretation that the stellar polytropic states with $n < 5$ and with $n > 5$ and $D < D_{\rm crit}$ are dynamical equilibrium states that are even stable with respect to a non-linear perturbation (Chavanis 2003; Chavanis & Sire 2004). In subsequent section, we report the results of the N-body simulations, which are carried out to investigate how the stellar polytrope actually evolves.

3 NUMERICAL SIMULATIONS

We are in a position to discuss the long-term dynamical evolution from the non-equilibrium N-body system and to explore the reality of stellar polytropes as quasi-equilibrium state. The N-body experiment considered here is the same situation as investigated in classic papers. That is, we treat the self-gravitating N-body system confined in an adiabatic wall of sphere. Hereafter, we set the units to $G = M = r_e = 1$ without loss of generality. According to the Antonov problem, all the particles are assumed to have the same mass $m = 1/N$, where N is the total number of the particles. The initial conditions for particle data were whole created by a random realization of the stellar models. To investigate the evolutionary states of the N-body system from the thermostatistical point-of-view, we deal with the three kinds of the stellar models: (i) isothermal distribution (ii) stellar polytropes and (iii) the stellar models with cuspy density profile. Table 1, 2 and 3 summarize the simulation runs, which are frequently referred in subsequent section. The generation of random initial data was basically followed by the rejection method described in Aarseth et al. (1974) (see also Chap.8 of Aarseth 2003). Using the analytic form of the mass profile $m(r)$ and the one-particle distribution function $f(\epsilon)$ as function of specific energy $\epsilon = v^2/2 + \Phi(r)$, this method generates the random distribution that possesses the same phase space structure as in the initial stellar model.

We are specifically concerned with collisional aspects of N-body dynamics, the timescale of which is much longer than the two-body relaxation time. For this purpose, we utilized a special-purpose hardware, GRAPE-6, which is especially designed to accelerate the gravitational force calculations for collisional N-body system (Makino et al. 2003). With this implementation, we use the fourth-order Hermite integration scheme with individual time-step algorithm, which is suitably efficient to combine with GRAPE-6 facility.

In our setup, the adiabatic wall is implemented by the same procedure as used by Endoh et al. (1997). The adiabatic wall reverses the radial components of the velocity for particles just located at the wall. Since we use an individual time-step algorithm, the positions of the particles are monitored at each fixed time interval ΔT, which is chosen to be a synchronized time interval in our time-step algorithm. This guarantees that the penetration of particles into the wall can be ignored. At these times, the radial components of velocities for particles outside the wall are reversed if the radial velocity vector is directed outward. Namely,

$$\boldsymbol{v} \longrightarrow \boldsymbol{v} - \frac{(\boldsymbol{v}\cdot\boldsymbol{x})}{|\boldsymbol{x}|}\ \frac{\boldsymbol{x}}{|\boldsymbol{x}|} \tag{26}$$

After particles were reversed, we recalculated the force and adjusted the time-step of particles.

Note that we did not use the regularization scheme to treat the close two-body or multiple encounter (e.g., Aarseth 2003). Because of the adiabatic wall, the standard scheme of regularization method is not directly applicable and the implementation of the regularization keeping the high accuracy requires a considerable amount of programming. Since we are interested in a quasi-equilibrium evolution before the core-collapse stage, absence of the regularization scheme itself is not crucial. Rather, a serious problem might arise from an introduction of the potential softening in order to reduce the numerical error. In general, the potential softening diminishes the close-encounter of each particle and it makes the energy exchange of the particles inefficient. This would lead to the overestimation of the relaxation timescales even before the core-collapse stage. In appendix A, the significance of the potential softening to the time-scale of core-collapse and/or quasi-equilibrium sequences is examined. Based on these experiments, we adopt the Plummer softened potential ($\phi = 1/\sqrt{r^2+\epsilon^2}$) and basically set the softening parameter to $\epsilon = 1/N$ when estimating the time-scale (Sec.4.2). Otherwise, we set $\epsilon = 4/N$ (Sec.4.1 and 4.3).[2]

4 RESULTS

In our present situation with units $G = M = r_e = 1$, the dynamical time given by roughly corresponds to $t_{\rm dyn} = (3\pi/16G\rho_0)^{1/2} \simeq 1$ and thus the global relaxation time becomes $t_{\rm relax} = 0.1(N/\ln N)\, t_{\rm dyn} \sim N/\ln N$. While this relation gives a crude estimate of the relaxation timescales, a more useful convention might be the half-mass relaxation time (e.g., Spitzer 1987; Binney & Tremaine 1987):

$$t_{\rm rh} = 0.138\ \frac{N}{\ln\Lambda}\left(\frac{r_{\rm h}^3}{GM}\right)^{1/2}, \tag{27}$$

where the Coulomb logarithm $\ln\Lambda$ is usually taken as $\ln\Lambda = \ln(0.4N)$ or $\ln(0.1N)$ (Spitzer 1987; Giersz & Heggie 1994). In what follows, adopting the latter convention ($\Lambda = 0.1N$), all the simulation results are presented by rescaling the timescale with the half-mass relaxation time evaluated at an initial time, $t_{\rm rh,i}$. In tables 1-3, half-mass radii for each initial distribution are evaluated and their numerical values are summarized.

4.1 Isothermal distribution

Let us first check our numerical calculations by examining the cases with isothermal initial conditions and comparing those results with previous work by Endoh et al. (1997), who have investigated the gravothermal expansion of the isothermal distribution under the same setup as examined in our simulation. Following their paper, we examine the three kinds of initial conditions, summarized in table 1.

Figure 3 and 4 respectively show the snapshots of evolved density profiles and one-dimensional velocity dispersion profiles starting from a stable initial configuration(*left*) and unstable initial distributions(*middle, right*). Here, the term, stable or unstable is used according to the initial density contrast D smaller or larger than the critical value $D_{\rm crit} = 709$, which is obtained from the thermostatistical prediction. The evolutionary path for each run is depicted in figure 2. In figure 3, while the evolved density profiles starting from the the stable initial condition is, by construction, stable and almost remain the same, the fate of the unstable cases sensitively depend on the randomness of the initial data, leading to the very different endpoints. The results depicted in the middle and the right panels of figure 3, both of which were started with the same initial parameters, are indeed such examples. Discriminating the final fate of the system from the initial random distributions seems generally difficult, however, the evolved density profiles seen in figure 3 are intimately connected with the response of the velocity structure shown in figure 4. Suppose that the velocity dispersion at the central part is initially higher than that at the outer part. In this case, the energy exchange by the two-body encounter yields the kinetic energy transport from the core to the halo. In other words, the outward heat flows occur and due to the negative specific heat, the inner part gets hotter, leading to the catastrophic growth of velocity dispersion. As a consequence, the core-collapse takes place. On the other hand, when the velocity dispersion at the inner part is relatively lower than that at the outer part, the inward heat flow conversely occur, which makes the core expand. In contrast to the former case, the heat flow can stop after balancing the thermal inertia at inner and outer parts. As a result, the system finally reaches the stable isothermal configuration. Though not clearly seen its signature, the response of the velocity dispersion profiles seen in figure 4 are consistent with the evolution of the density profiles. Compared the results in the unstable cases with the results obtained by Endoh et al. (1997), the resultant density profiles are similar and the evolved timescales for the unstable cases almost agree with each other.

As for the stable case, a calculation was proceeded up to $t = 112t_{\rm rh,i}$, corresponding to $t = 2000$ in unit of N-body time, which was longer calculation time than that of the other runs. A closer look at figure 3 shows that the central density slightly increases and the system seems to become out of equilibrium. The total energy of the system was conserved to 0.05% at the end of the calculation, which is relatively larger value than the errors in the other runs. Thus the destabilization of the core

[2] Hereafter, the quantity ϵ is interchangeably used to imply the specific energy of a particle and the softening length. Readers should not confuse the meanings of ϵ.

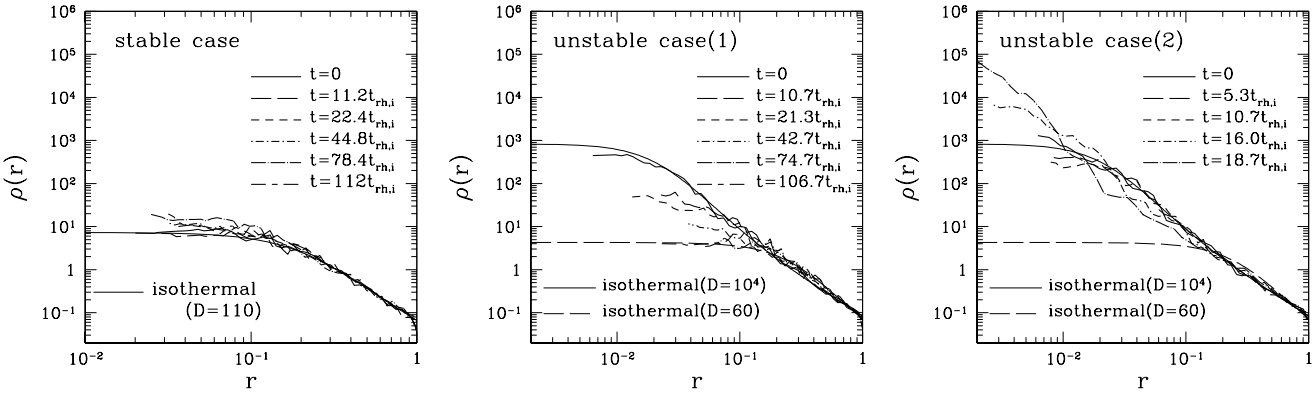

Figure 3. Snapshots of density profile in the stable case(*Left*) and the unstable cases(*Middle* and *Right*). In each panel, the thick lines represent the snapshots of simulation results, while the thin lines indicate the ones obtained from the Emden solutions of isothermal distribution.

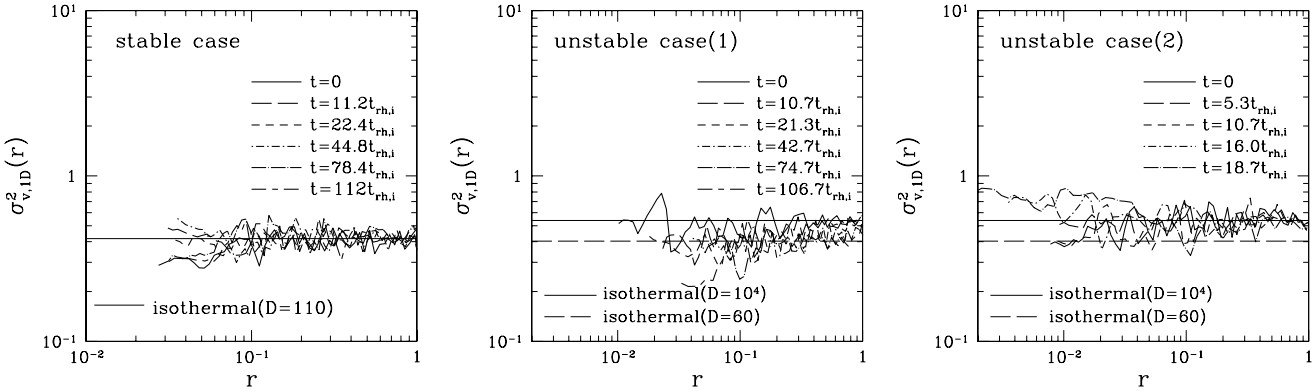

Figure 4. Snapshots of one-dimensional velocity dispersion profile in the stable case(*Left*) and the unstable cases(*Middle* and *Right*).

Table 1. Model parameters of initial condition in the case of the isothermal distribution

run #	parameters	half-mass radius($r_{\rm h}/r_e$)	# of particles	status
stable	$D = 110$	0.4834	2k	stable
unstable1	$D = 10^4$	0.4993	2k	expansion
unstable2	$D = 10^4$	0.4993	2k	collapse

may be attributed to the numerical error in the energy conservation. Though the effect of destabilization yields a serious problem in estimating the time scale of core-collapse, we are specifically concerned with the evolutionary sequence before entering the core-collapse phase. Hence, at a level of this present accuracy, one can ignore the destabilization effect as long as the total energy of the system is well conserved.

4.2 Stellar polytropes

Having checked the validity of the numerical calculations, we next investigate the non-equilibrium evolution away from the isothermal equilibrium state. In this subsection, we deal with a class of initial conditions characterized by the stellar polytropes. Table 2 summarizes the model parameters of initial distributions. The evolutionary track for each run is depicted in the energy-density contrast relation in figure 2.

Overall behaviors of the simulation results are as follows. Before entering the core-collapse stage, most of the system experiences the quasi-equilibrium stage, in which the distribution function slowly changes in time. The evolutionary sequence in the quasi-equilibrium stage can be well-approximated by the one-parameter family of stellar polytropes with the time-varying polytrope index. Apart from some fluctuations, the fitted value of the polytrope index, on average, increases monotonically with time, implying that the system tends to approach the exponential distribution.

To see the quasi-equilibrium behavior quantitatively, we first show the representative result obtained from the run $n3A$,

Table 2. Model parameters and the evolutionary states in the cases starting from the stellar polytropes

run #	model parameters	half-mass radius($r_{\rm h}/r_e$)	# of particles	realizations	fitting to stellar polytrope
n3A[1]	$n=3$, $D=10^4$	0.3282	2k, 4k, 8k	2, 1 ,1	successful
n5A	$n=5$, $D=10^2$	0.4611	2k	2	successful
n5B	$n=5$, $D=10^3$	0.3114	2k	3	successful
n5C	$n=5$, $D=10^4$	0.2025	2k	2	successful
n5D	$n=5$, $D=10^6$	0.08196	2k	2	failed
n6A[2]	$n=6$, $D=110$	0.4531	2k	1	successful
n6B[3]	$n=6$, $D=10^4$	0.1794	2k	1	successful

[1] initial distribution corresponding to *run A* in Taruya & Sakagami (2003c)
[2] initial distribution corresponding to *run B1* in Taruya & Sakagami (2003c)
[3] initial distribution corresponding to *run B2* in Taruya & Sakagami (2003c)

i.e., the stellar polytrope with index $n=3$ and with the initial density contrast $D=10^4$. Then we discuss the other runs, $n5A \sim n5D$ and $n6A, B$ in section 4.2.2.

4.2.1 run n3A

Figure 5 shows the time evolution of the Lagrange radii taken from the run with $N=2K$, plotted as function of time in unit of the half-mass relaxation time. With the softening parameter $\epsilon = 1/N$, the core-collapse takes place at $t \sim 44 t_{\rm rh,i}$ and the core-halo structure was developed at the end of the calculation. Looking at an earlier phase, the Lagrangian radii evolve very slowly and one can clearly distinguish the timescales between the early relaxation phase and the late-time core-collapse phase. Since the early stage of the time evolution seems nearly equilibrium, we will especially call it quasi-equilibrium evolution. In a quasi-equilibrium regime, while decreasing the inner Lagrangian radii, the outer Lagrangian radii slightly expands to compensate the slow contraction of the core.

To see the quasi-equilibrium structure in more detail, in figure 6, we plot the snapshots of the density profile as function of radius (*left*), the distribution function as function of specific energy of the particles $\epsilon = v^2/2 + \Phi(r)$ (*middle*) and the velocity dispersion profile as function of radius (*right*) during the quasi-equilibrium regime. In each panel, the symbols denote the simulation results. Note that for clarify, the results are offset vertically, successively by two-digits below, except for the final output at $t = 30 t_{\rm rh,i}$.

In figure 6, the solid lines show the initial stellar polytrope with $n=3$ evaluated from the Emden solutions. Comparing those curves with simulation results, one deduces that the system at an earlier time is slightly out of equilibrium and it gradually deviates from the initial state. While the velocity dispersion profile monotonically increases at an outer part, the density profile first increases at both the inner and the outer parts ($t \lesssim 5 t_{\rm rh,i}$), leading to a slight decrease of the density contrast $D = \rho_c/\rho_e$ (see the arrow labeled by *n3A* in figure 2). Later, the increase of the core density surpasses that of the edge density and thereby the density contrast turns to increase ($t \gtrsim 10 t_{\rm rh,i}$).

In figure 6, in order to characterize the evolutionary sequence of the quasi-equilibrium state, the simulation results are compared with a sequence of the stellar polytropes. The fitting results are then plotted as long-dashed, short-dashed, dot-dashed and dotted lines from the data at $t = 5 t_{\rm rh,i}$ to that at $t = 30 t_{\rm rh,i}$. In fitting the simulation data to the stellar polytropes, we first quantify the radial density profile $\rho(r)$ from each snapshot data. Selecting the 100 points from it at regular intervals in logarithmic scale of radius r, the results are then compared with the Emden solutions. [3] Note that in our present situation, the total energy and the mass are conserved. Thus, the only fitting parameter is the polytrope index. We determine the index n so as to minimize the function χ^2:[4]

$$\chi^2(n) = \sum_{i=1}^{100} \left\{ \frac{\rho_{\rm sim}(r_i) - \rho_{\rm Emden}(r_i; n)}{\rho_{\rm sim}(r_i)} \right\}^2 , \tag{28}$$

Clearly from figure 6, the stellar polytropes quantitatively characterize the evolutionary sequence of the simulation results. Note that we obtained $\chi^2 \simeq 4$–8 for each time-step, indicating that the fitting result is satisfactory. A closer look at the low-energy part of the distribution function $f(\epsilon)$ reveals that the simulation results partly resemble the exponential form rather than the power-law function. Nevertheless, the most remarkable fact is that the stellar polytropes as simple power-law distribution globally approximate the simulation results in a quite good accuracy. Moreover, the fitting results in

[3] Reason why we adopted the density profile instead of the distribution function is that the density profile can be very sensitive to the dynamical evolution process. Further, in spherically symmetric and isotropic cases, the density profile is uniquely determined from the distribution function through the Eddington formula (Binney & Tremaine 1987). Thus, in the present situation, it seems better to perform the fitting by using the radial density profile.
[4] Strictly speaking, this is not the χ^2 function usually used in the likelihood analysis.

figure 6 indicate that the fitted values of the polytrope index monotonically increase in time, in contrast to the non-monotonic behavior of the density contrast. In order to quantify the evolution of polytrope index, we collect the new snapshot data at each time interval $\Delta t = 10$ in N-body units for the run with $N = 2K$. Repeating the same fitting procedure as in figure 6, the polytrope indices are estimated at each time step and the resultant values are plotted in figure 7 together with the χ^2 value of the fitting results. Here we also plot the results obtained from the run with $N = 4K$ and $N = 8K$, in which the time intervals are respectively chosen as $\Delta t = 20$ and 50.

Clearly, the fitted values of the polytrope index monotonically increase apart from the fluctuations during the short time interval. The growth rates of the polytrope index normalized by half-mass relaxation time almost coincide with each other, consistent with the fact that the quasi-equilibrium sequence is evolved via two-body relaxation. In upper panel of figure 7, the horizontal dotted line denote the critical index $n_{\rm crit}$, corresponding to the point at which $d\lambda/dD = 0$ for a given λ in $(\lambda,\ D)$-plane. According to the prediction from the non-extensive thermostatistics with Tsallis entropy, after reaching the critical index $n_{\rm crit}$, the system is expected to enter the gravothermally unstable regime. That is, the relaxation timescales between the inner and the outer parts are decoupled and the system finally undergoes the core-collapse. In a rigorous sense, the thermodynamic prediction itself cannot be applicable to the out-of-equilibrium state, however, it turns out that the predicted value $n_{\rm crit}$ or $D_{\rm crit}$ is consistent with the N-body results. In fact, the successful fit is obtained until $t \simeq 34 t_{\rm rh,i}$, while the core-collapse takes place lately at $t \sim 44 t_{\rm rh,i}$ (see Fig.5). Thus, the prediction based on the non-extensive thermostatistics may provide a crude estimate of the boundary between the stability and the instability in the general non-isothermal states. This point will be further discussed in other runs.

4.2.2 Other runs

Figures 8–11 show the snapshots of the density profile, the distribution function and the velocity dispersion profile obtained from the runs $n5A$–$n5D$, which were all started with the same polytrope index $n = 5$, but with the different initial density contrasts; $D = 100$(run $n5A$, Fig.8): $D = 10^3$(run $n5B$, Fig.9), $D = 10^4$(run $n5C$, Fig.10) and $D = 10^6$(run $n5D$, Fig.11). Also in figures 13 and 14, the results taken from the runs $n6A$ and $n6B$ are depicted, whose initial density contrasts are $D = 110$ and 10^4, respectively.

Similarly to the run $n3A$, the results from the runs $n5A$–$n5C$, $n6A$ and $n6B$ exhibit the quasi-equilibrium regime in the early phase of the evolution. The evolutionary sequences in the quasi-equilibrium regime can be quantitatively characterized by a family of stellar polytropes with time-dependent polytrope index. Figures 12 and 15 summarize the fitting results for polytrope index as function of time in logarithmic scales. It seems apparently that for the cases starting with smaller value of D (i.e., runs $n5A$ and $n6A$), time variation of polytrope index is systematically large and statistical fluctuation become noticeable, however, it turns out that this fact simply comes from the geometrical reason for the equilibrium sequence plotted in figure 2. That is, in $(\lambda,\ D)$-plane, a number of trajectories of the stellar polytropes with different polytrope index n are assembled at the narrow region with smaller value, D or λ, causing a large variation and/or fluctuation in the time evolution of polytrope index.

Apart from this behavior, figures 12 and 15 show that the timescales of quasi-equilibrium state crucially depend on the initial conditions, which are basically characterized by the initial density contrast D or the dimensionless energy λ. Qualitatively, the timescale of quasi-equilibrium state is understood from the local estimates of the relaxation time, which are inversely proportional to the local density (e.g., Spitzer 1987; Binney & Tremaine 1987):

$$t_r = 0.065\ \frac{v^3}{G^2 m\, \rho\ \ln\Lambda}. \tag{29}$$

For a system with small initial density contrast, the depth of the potential becomes shallower and equation (29) implies that the relaxation proceeds slowly enough in both core and halo. The quasi-equilibrium state is thus expected to be long-lived. As anticipated in figures 8 and 13, fitting to the stellar polytropes is successful until $t \simeq 63 t_{\rm rh,i}$ for run $n5A$ and $66 t_{\rm rh,i}$ for run $n6A$, much longer than the other cases.

On the other hand, for a system with large initial density contrast, equation (29) suggest that the decoupling of the timescales between core and halo would occur earlier and the quasi-equilibrium phase would be short-lived. Indeed, the distribution functions for runs $n5C$ and $n6B$ show that while the high-energy part of the function $f(\epsilon)$ almost remains the same, the low-energy part of the distribution is rapidly developed and stretches toward $\epsilon \to -\infty$. Also, the inner part of the density profile grows rapidly and shows an intermittent behavior with large fluctuation. As a result, fitting to the stellar polytropes failed earlier at $t \sim 20 t_{\rm rh,i}$ for run $n5C$ and $12 t_{\rm rh,i}$ for run $n6B$. After that, the system soon becomes unstable state, finally undergoing the core-collapse, consistent with the thermodynamic prediction based on the Tsallis entropy. Note that the fitting results in the runs $n5C$ and $n6B$ are slightly worse. From bottom panels of figures 12 and 15, the estimated χ^2 values given by (28) become $5 \sim 14$ in both runs, which is larger than the typical value $3 - 7$ in cases with the smaller initial density contrast.

The observation in both fitting results and the timescales for quasi-equilibrium states indicates that for some large values of the initial density contrast, the fitting to stellar polytropes would fail from the beginning and the quasi-equilibrium state ceases to exist. Indeed, such an example was obtained from the run $n5D$ (see Fig.11). The initial density contrast of this run is $D = 10^6$ and the dimensionless energy is $\lambda = 2.345$. That is, the location of the initial state in the (λ, D)-plane is outside the region depicted in figure 2. In this case, the central part of the system is highly concentrated and the core-halo structure is developed from the beginning. The resultant relaxation timescale is much shorter than that of the other cases

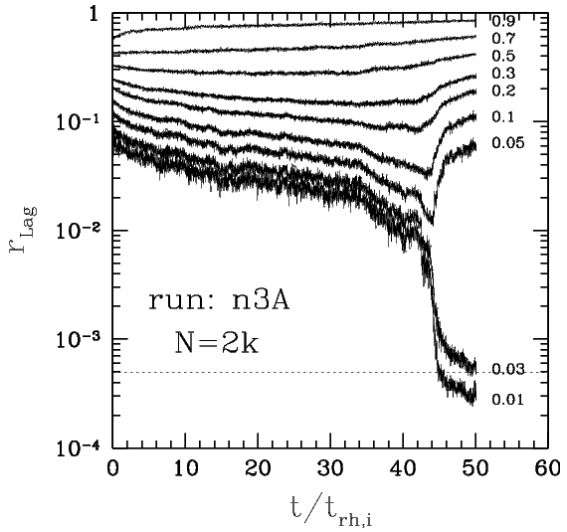

Figure 5. Lagrangian radii as function of time obtained from the run *n3A*. Each line represent the radius of the shell which contains a constant mass fraction. The numerical values of the mass fraction are indicated in the right part of figure. The horizontal dotted line is the potential softening scale, $\epsilon = 1/N \simeq 4.9 \times 10^{-4}$.

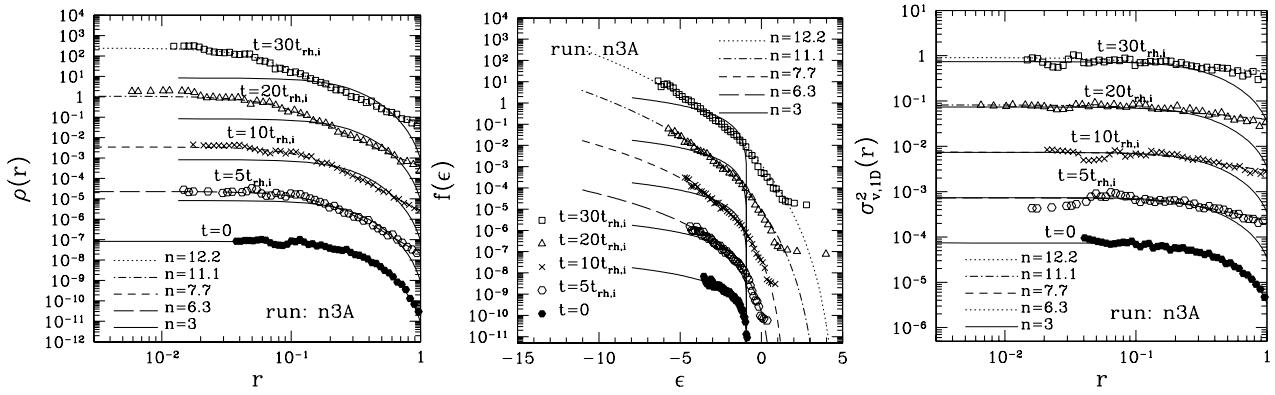

Figure 6. Snapshots of density profile $\rho(r)$ (*Left*), distribution function $f(\epsilon)$ as function of specific energy of particles $\epsilon = v^2/2 + \Phi(r)$ (*Middle*) and one-dimensional velocity dispersion $\sigma^2_{\rm v,1D}(r)$ (*Right*) from the run *n3A*. In each panel, symbols represent the N-body results, while the solid lines show the Emden solutions of initial distribution. The lines except for the solid lines are the results fitted to the one-parameter sequence of stellar polytropes. Note that for clarify, the results are offset vertically, successively by two-digits below, except for the final output.

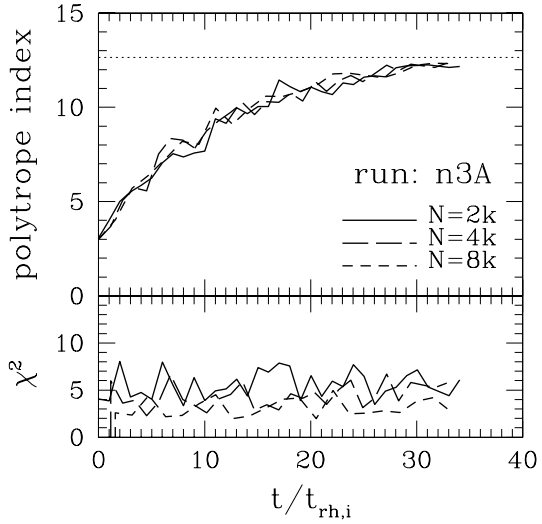

Figure 7. Time evolution of polytrope index fitted to the N-body simulations in the case of the run *n3A*. The upper panel shows the fitting results for the runs with particles $N = 2,048$(*solid*), $4,096$(*long-dashed*) and $8,192$(*short-dashed*). The horizontal dotted line represents the critical index $n_{\rm crit}$, corresponding to the marginal state of the entropy S_q satisfying the condition $d\lambda/dD = 0$ in the case of run *n3A*. The lower panel represents the goodness of fit by plotting the function χ^2 defined in equation (28).

and the system soon becomes unstable, leading to the earlier core-collapse. Compared to the stable stellar polytropes with the same initial energy $\lambda = 2.345$ and with $D < D_{\rm crit}$, none of the model parameters successfully reproduce the simulated density and/or velocity dispersion profiles (long-dashed, short-dashed and dot-dashed lines in Fig.11). Though the collapse time crucially depends on the softening parameter, the convergence test as examined in appendix A suggests that the collapse time converges to $18t_{\rm rh,i}$, close to the standard result without the adiabatic wall, i.e., $t_{\rm coll} \simeq 16t_{\rm rh,i}$ (e.g., Table13.2 of Aarseth 2003).

Therefore, for a general initial condition with large D or λ, quasi-equilibrium behavior generally ceases to exist. In other words, long-lived quasi-equilibrium states appear at the smaller value of λ or D and the system is quantitatively characterized by the stellar polytropes. Their lifetime is expected to become much longer as approaching down to $\lambda = 0.335$ and/or $D = 709$, i.e., the critical values for the marginal stability in isothermal distribution.

4.2.3 Discussion

So far, we have focused on the characterization of the quasi-equilibrium state using the one-parameter family of the stellar polytropes. While most of the transient state is well-approximated by the stellar polytropes with varying polytrope index, one may criticize that the use of the stellar polytropes is not the best characterization for the quasi-equilibrium sequence. Indeed, even restricting the stellar distribution to the stationary solutions of the Vlasov equation, one can, in principle, construct the infinite set of one-parameter family of stellar models. In this sense, the stellar polytropes should be regarded as a particular set of stellar models. Further, there is no rigorous proof for the uniqueness to characterize the quasi-equilibrium states.

In real astronomical systems such as globular clusters, the stellar polytropes had been known to poorly fit to the observed structure of stellar distribution. Rather, the majority of the Galactic globular clusters is quantitatively characterized by the King model (King 1966; Binney & Tremaine 1987; Spitzer 1987; Meylan & Heggie 1997). In contrast to the stellar polytropes as *q-exponential* distribution, King model is represented by the *truncated* exponential distribution:

$$f(\epsilon) \propto \begin{cases} e^{-\beta\epsilon'} - 1 & ; \quad \epsilon' < 0 \\ 0 & ; \quad \epsilon' \geqslant 0 \end{cases}, \tag{30}$$

where we define $\epsilon' = \epsilon - \phi(r_B)$ with radius r_B being the truncation radius and ϵ is the specific energy of a particle. Provided the dimensionless energy λ, the equilibrium sequence of the King model is then characterized by the one-parameter $W_0 = 2\beta[\phi(r_B) - \phi(0)]$, which represents the depth of the gravitational potential.

In figure 16, the N-body data taken from the run $n3A$ is used to compare with the King model. Note that the fitted values of the parameter W_0 indicated by figure 16 were obtained under the suitable restriction, $r_B > r_e$. Similar to the stellar polytropes, the density and the velocity dispersion profiles reasonably fit to the King model. The fitted value of the parameter W_0 gradually increases as time goes on, indicating that the depth of the potential becomes deeper. Compared with the observed Galactic globular clusters with typical range $W_0 = 4$–10 (Trager et al. 1995), fitting results for W_0 are somewhat large.

On the other hand, turn to focus on the distribution function, deviation from the King model becomes manifest at the high-energy tails $\epsilon > 0$. While the distribution function for King model falls off at the truncation energy $\epsilon = \phi(r_B)$ which takes the negative value, number of high-energy particles with $\epsilon > 0$ gradually increases in our N-body calculation, which contributes to a high-energy tail of the distribution function. Although the low-energy part of the distribution function resembles the exponential form of the King model, the discrepancy at the high-energy part implies that the boundary condition in our idealistic situation is very different from that of the Galactic globular clusters. In fact, the influence of external tidal field is significant for the Galactic globular cluster and the resultant distribution function sharply falls off at the tidal boundary (Binney & Merrifield 1998). The stellar particles which are usually bounded to the system tend to escape from the globular cluster system (e.g., Fukushige & Heggie 1995; Baumgardt & Makino 2003; Tanikawa & Fukushige 2005). To mimic this effect, truncation radius r_B is artificially introduced by hand in the King model. On the other hand, in presence of the adiabatic wall, the high-energy particles with $\epsilon > 0$, which are usually unbounded, cannot freely escape outward from the system and thereby no specific energy cutoff appears.

As a result, the stellar polytropic distribution which has no energy cutoff successfully reproduces the quasi-equilibrium states in our N-body setup. This means that, in presence of the adiabatic wall, the simple power-law distribution provides a better characterization than the truncated exponential distribution. Since the adiabatic wall is an artificial but the simplest boundary condition, the stellar polytropic distribution might be regarded as a fundamental stellar model theoretically, though not practically useful in characterizing the observed structure of Galactic globular clusters.

4.3 A family of stellar models with cusped density profile

The analyses in previous subsection have revealed that the quasi-equilibrium evolution characterized by the stellar polytropic distribution can appear at the energy λ close to the critical value of the isothermal distribution. We then attempt to clarify the generality and/or the physical conditions for the quasi-equilibrium state in more general initial conditions. In this subsection, as a special class of initial conditions that contain the non power-law features, we treat a family of stellar models with cusped density profile (Tremaine et al. 1994). The models contain two parameters, one is the scale-radius a, and the other is related to the slope of the inner density profile η. The density profiles of these models are expressed as:

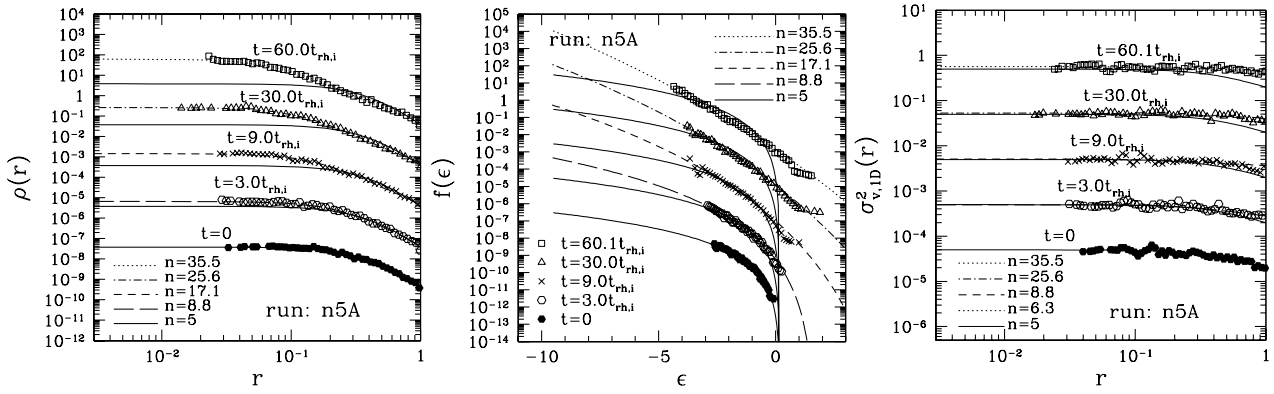

Figure 8. Snapshots of the density profile, distribution function and the velocity dispersion profile from the run $n5A$

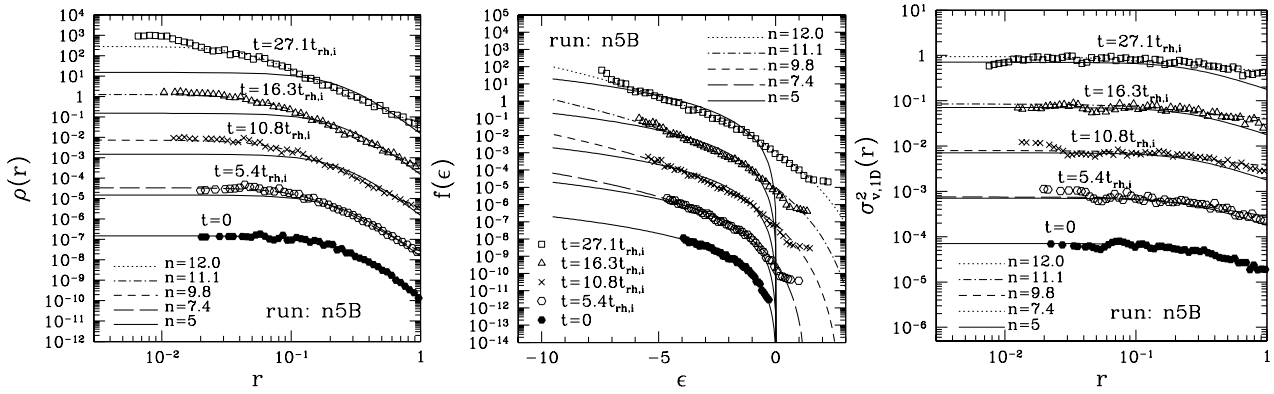

Figure 9. Same as Fig.8, but in case of the run $n5B$.

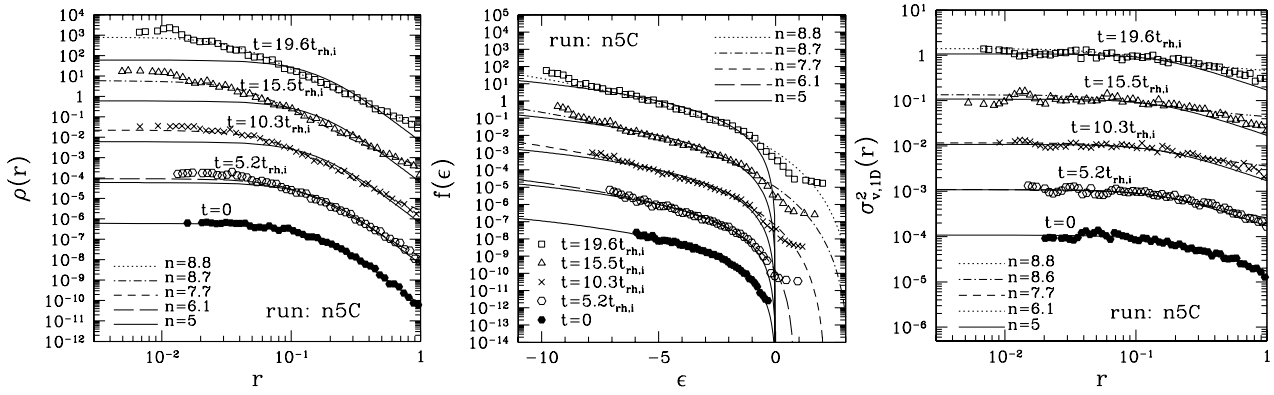

Figure 10. Same as Fig.8, but in case of the run $n5C$.

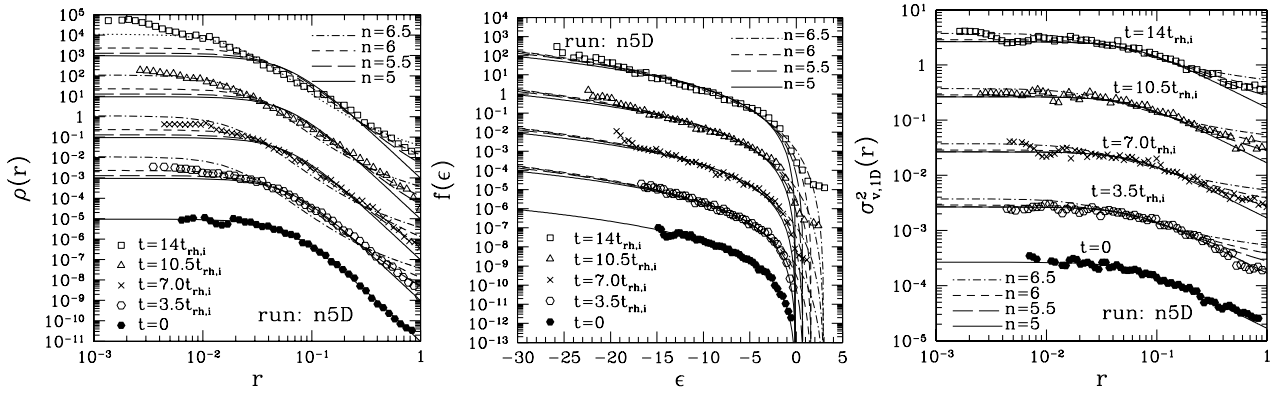

Figure 11. Same as Fig.8, but in the case of the run $n5D$.

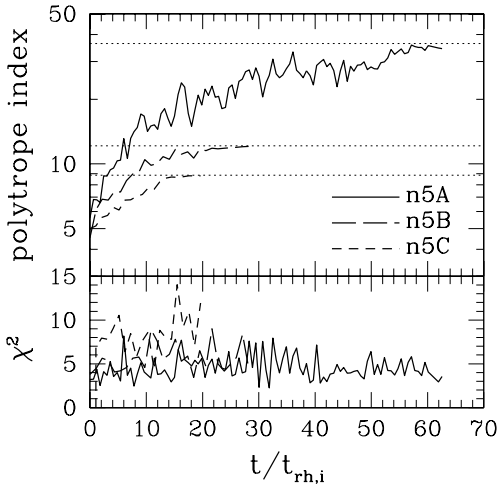

Figure 12. Evolution of polytrope index in the runs $n5$A, $n5$B and $n5$C.

$$\rho(r) \propto \frac{1}{(r/a)^{3-\eta}(1+r/a)^{1+\eta}}. \tag{31}$$

Note that the above expression includes the models considered by Hernquist (1990) for $\eta = 2$ and by Jaffe (1983) for $\eta = 1$ as special cases.

4.3.1 N-body setup and overview

For a spherically symmetric configuration with isotropic velocity distribution, using the Eddington formula, the one-particle distribution function can be uniquely reconstructed from the density profiles (31) (Binney & Tremaine 1987). Tremaine et al. (1994) gave useful analytic formulas for various physical quantities such as the distribution function, the potential and the velocity dispersion profiles for a system extending over the infinite radius, $r \to \infty$. Based on their formulas, Quinlan (1996) numerically estimated the dependence of the slope η on the timescale of core-collapse using the Fokker-Planck code. For present purpose, however, a direct application of their formulas is inadequate in presence of the adiabatic wall.

In appendix B, taking account of the truncation radius r_e, we re-derive the analytic formulas for distribution functions as well as the other physical quantities. Based on this, figure 17 plots the theoretical curves for the distribution function(*left*) and the velocity distribution profile(*right*) with a specific choice of the parameters, $\eta = 1$, 1.5, 2 and 3, fixing the scale-radius to $a/r_e = 0.5$. For models with $\eta > 1$, the distribution function exhibits a divergent behavior at a finite energy $\epsilon = \epsilon_{\rm min} < 0$, $f(\epsilon_{\rm min}) = +\infty$. Further, the velocity dispersion profile shows non-monotonic behavior; it first increases and eventually turns to decrease as approaching the center. These peculiar features imply that the inward heat flow occurs along a course of the relaxation, causing the central part of the system expand, which is the same phenomenon as observed in the unstable case of the isothermal distribution (see Sec.4.1).

To perform a simulation, we increased the number of particles to $N = 8K$ in order to resolve the central part of the cuspy density profiles. The softening parameter of gravitational potential is set to $\epsilon = 4/N$. Note that the convergence test in appendix A suggests that much smaller value of the softening parameter should be used for a system with highly concentrated core. However, decreasing the softening parameter requires a much longer calculation time and the probability of binary-formation via three-body interaction increases around the core. Since we use a simple individual time-step algorithm without any regularization schemes, the N-body integration becomes heavily time-consuming once a tight binary is formed. Hence, we do not discuss here the timescale of the quasi-equilibrium state and focus only on the condition for quasi-equilibrium states. The quantitative estimates of the timescale will be presented in future task.

In table 3, the model parameters of the initial conditions examined here are summarized, together with the evolutionary status. Also in figure 18, the result for each run is represented by the symbols in energy-scale radius relation. Roughly speaking, figure 18 says that the quasi-equilibrium sequence characterized by the stellar polytrope appears(*open stars*, case(B)) when the total energy of the system is not far from the critical energy of isothermal distribution, $\lambda_{\rm crit} = 0.335$. However, this is not a sufficient criterion for the presence of quasi-equilibrium state. For models with $\eta = 1$, whose density profile resembles a singular isothermal sphere at the center, the system cannot be fitted by the stellar polytrope (*filled stars*, case(A)). On the other hand, for the initial conditions with $\lambda < \lambda_{\rm crit}$ (*stars* in shaded-region), the system finally approaches the isothermal state. In this case, the transient state of the system could be also fitted by the stellar polytropes, although the fitted value of the polytrope index is so large that one cannot be easily discriminate it from the isothermal distribution.

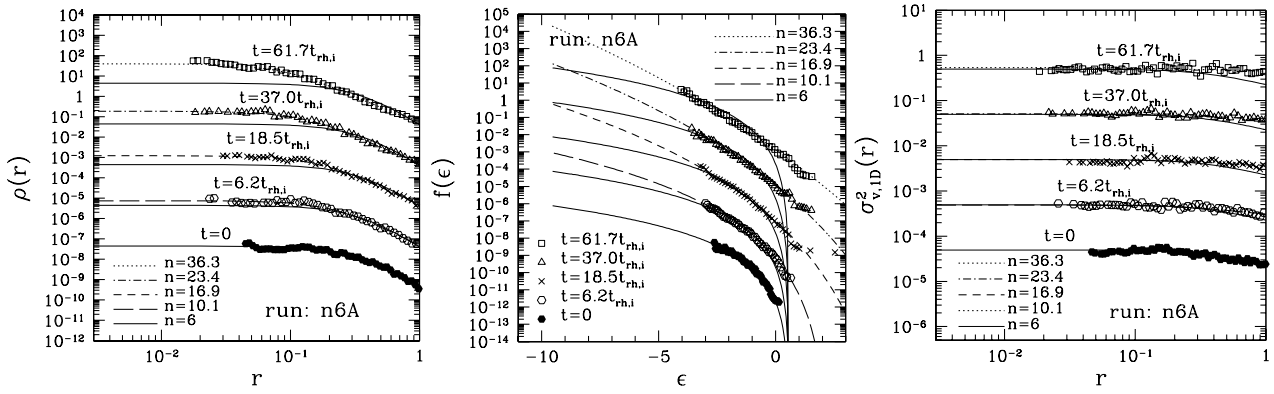

Figure 13. Same as Fig.8, but in the case of the run $n6A$.

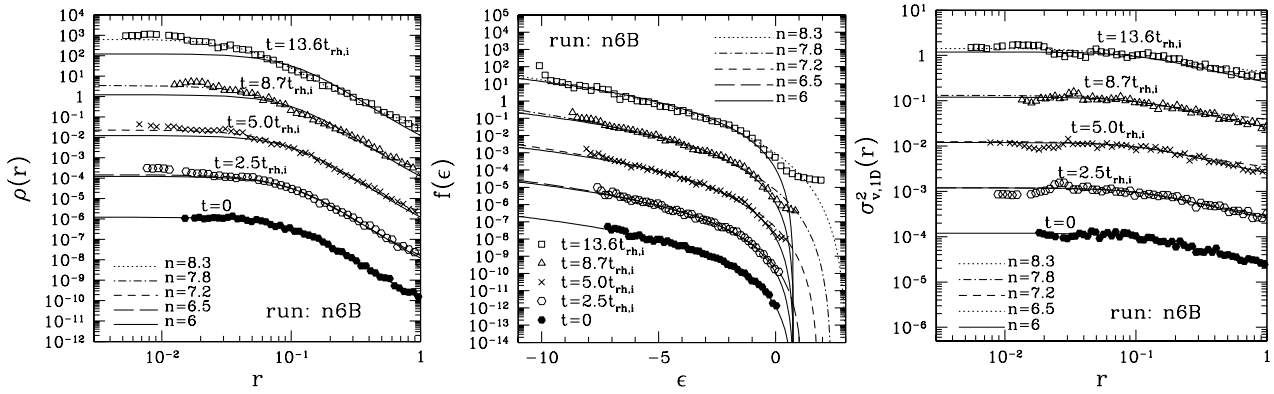

Figure 14. Same as Fig.8, but in the case of the run $n6B$.

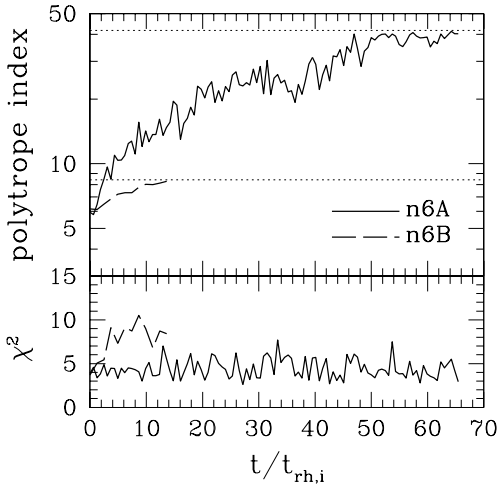

Figure 15. Evolution of polytrope index in the cases of runs $n6$A and $n6$B

4.3.2 quasi-attractive behaviors and condition for quasi-equilibrium state

Let us focus on the characteristic behaviors of the long-term evolution by picking up some typical examples. Figures 19, 20 and 21 show the results obtained from the runs $\eta 2C$, $\eta 1.5B$ and $\eta 1C$. Figure 19 shows the typical example in which the system finally approaches the stable isothermal state. Due to the small value of λ, the effect of self-gravity is small and the system evolves very slowly. While we tried to fit the transient states of the system to the stellar polytropes, the resultant value of the polytrope index n is quite large, $n \simeq 20$–60, indicating the system being in nearly isothermal state. For comparison, we also plot the theoretical curves for isothermal distribution. It seems difficult to discriminate which models are fitted to the simulation results better.

By contrast, in figure 20, the quasi-equilibrium state approximated by the stellar polytropes appears. In the run $\eta 1.5B$, because of the dimensionless energy $\lambda > 0.335$, the system finally undergoes core-collapse. Looking at an early phase, however, the core expansion first takes place and the flatter core is formed. Then the core density turns to increase gradually and the

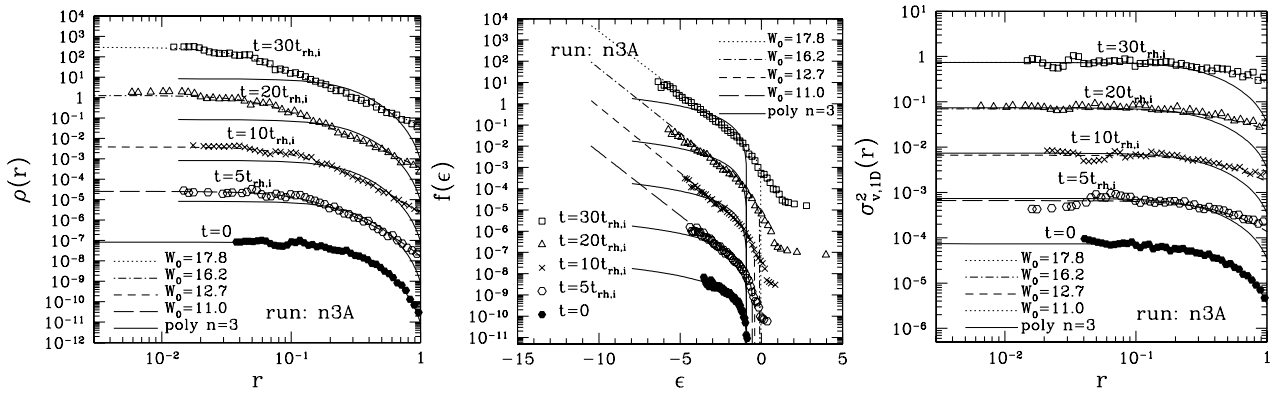

Figure 16. Same as Fig.6, but results are compared with the King models. The fitting results shown in the lines except for solid lines are obtained by varying the dimensionless parameter, $W_0 = 2\beta[\phi(r_B) - \phi(0)]$ under keeping the mass and the total energy fixed.

transient state can be approximately described by the stellar polytropes for a long time ($t \lesssim 30t_{\rm tr,i}$). These behaviors, which may be regarded as quasi-attractive behavior, can be explained from the inner structure of the initial velocity dispersion profile. That is, due to the small value of the local relaxation time t_r at the core, the inward heat flow first occurs toward the equipartition of the kinetic energy, leading to the uniform velocity dispersion at the inner part. Then, the outward heat flow next occurs and the inhomogeneity in the velocity dispersion is gradually erased. Although this slow relaxation does not stop and finally leads to the catastrophic heat flow, the system is remarkably long-lived.

On the other hand, the run $\eta 1C$ has slightly smaller value of λ than the run $\eta 1.5B$ and one naively expects that the system is stable. However, the results shown in figure 21 is completely opposite. In contrast to the run $\eta 1.5B$, the initial condition of the run $\eta 1C$ has uniform velocity dispersion at the inner part. This implies that the inward heat flow is only supplied by the randomness of the initial perturbation, as seen in the unstable isothermal case (see Sec.4.1). Thus, the amount of the heat flow is insufficient and the resultant core radius is rather small, whose density profile cannot be approximated by the stable stellar polytropic distribution. For comparison, in figure 21, we plot the stellar polytrope with index $n \simeq 17.6$, which is the marginal stable state that has the same total energy λ as in the run $\eta 1C$. While the distribution function and the velocity dispersion profile resemble the marginal stable state of the stellar polytrope, the discrepancy is manifest in the density profile. As a result, the system is short-lived and could not reach the quasi-equilibrium state.

Note that the lifetime in the model $\eta 1C$ sensitively depends on the randomness of the initial perturbation. Figure 21 shows the run-by-run variation of the time evolution of the core radii, where the core radius was estimated according to the procedure given by Casertano & Hut (1985) (see also Fukushige & Heggie 1995). Compared to the runs $\eta 2C$ and $\eta 1.5B$, the run-by-run variation in $\eta 1C$ is significant and it seems to originate from the first stage of the core expansion. This behavior also holds for the other runs $\eta 1A$ and $\eta 1B$. Therefore, the lifetime of the system starting from the initial conditions with cusped density profile $\rho \propto r^{-2}$ would be generally stochastic. Although the present calculation with non-zero softening parameter is inadequate to estimate the precise core-collapse time, the uncertainty of the collapse time would remain true even if the appropriate regularization scheme is implemented in our code. In other words, the condition for quasi-equilibrium state as well as the lifetime of the system are much sensitive to the velocity structure of the initial condition. Though the present surveys do not give a conclusive statement for generality of quasi-equilibrium state, the out-of-equilibrium state with the cusped profile $\rho \propto r^{-\alpha}$, $(\alpha < 2)$ possibly exhibits the quasi-equilibrium behaviors if the dimensionless energy λ is close to 0.335.

4.3.3 Entropy growth and quasi-equilibrium state

In order to elucidate the sequence of the quasi-equilibrium evolution from a thermodynamic point-of-view, we quantify the entropy growth for the N-body data, $\eta 2C$, $\eta 1.5B$ and $\eta 1C$. Though the quasi-equilibrium behavior seen in the simulations may imply that the entropy growth can be better characterized by the non-extensive Tsallis entropy, the entropy measure in quantifying S_q is not, strictly speaking, unique when comparing with different values of the polytrope indices n, or equivalently, the q-parameters. Therefore, as long as the cases with time-varying polytrope indices are concerned, it would be natural to quantify the entropy growth with the Boltzmann-Gibbs entropy.

In left panel of figure 23, the results are plotted as the trajectories in (D, $S_{\rm BG}/N$)-plane, together with the equilibrium sequence for the stellar polytropes denoted by continuous lines. The derivation of theoretical curves for isothermal and the stellar polytropes is described in appendix C. Also, in right panel, the entropy growth is quantified and is plotted as function of time. Note that the time interval between the symbols marked along each trajectory roughly corresponds to a half-mass relaxation time for the initial distribution.

In figure 23, while the time evolution of density contrast D shows non-monotonic behaviors, the specific entropy $S_{\rm BG}/N$ monotonically increases in time, consistent with the law of thermodynamics indicated by the Boltzmann H-theorem. The evolutionary sequence in the $(D, S_{\rm BG}/N)$-plane depends on the initial condition. In the case of the run $\eta 2C$, the left panel

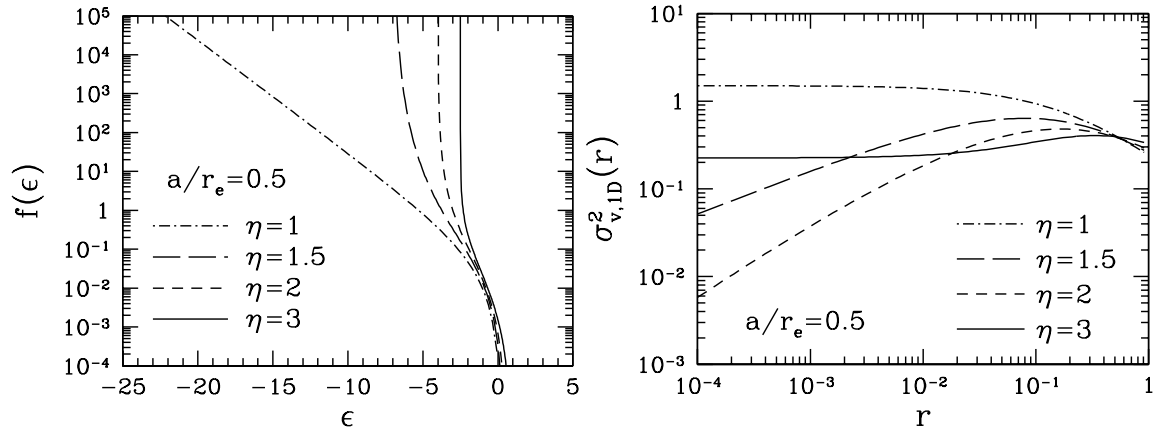

Figure 17. Distribution function(*Left*) and velocity dispersion profile(*Right*) for a family of stellar model by Tremaine et al. (1994) in presence of an adiabatic wall. For a specific value of the scale radius $a/r_e = 0.5$, the analytic results with various slopes η are plotted based on the formulae in Appendix B.

Table 3. Model parameters and the evolutionary states in cases starting from the stellar models by Tremaine et al. (1994).

run #	parameters	half-mass radius($r_{\rm h}/r_e$)	# of particles	realizations	transient state	final state
η1A	$\eta = 1$, $a/r_e = 0.5$	0.25	8k	2	none	collapse
η1B	$\eta = 1$, $a/r_e = 0.8$	0.3077	8k	6	none	collapse
η1C	$\eta = 1$, $a/r_e = 2.0$	0.4	8k	4	none	collapse
η1.5A	$\eta = 1.5$, $a/r_e = 0.2$	0.221	8k	2	none	collapse
η1.5B	$\eta = 1.5$, $a/r_e = 0.5$	0.362	8k	3	stellar polytrope	collapse
η1.5C	$\eta = 1.5$, $a/r_e = 1.0$	0.4598	8k	3	stellar polytrope	collapse
η2A	$\eta = 2$, $a/r_e = 0.2$	0.2869	8k	2	none	collapse
η2B[1]	$\eta = 2$, $a/r_e = 0.5$	0.4459	8k	2	stellar polytrope	collapse
η2C[2]	$\eta = 2$, $a/r_e = 1.0$	0.5469	8k	3	none	isothermal
η3A	$\eta = 3$, $a/r_e = 0.2$	0.3907	8k	2	stellar polytrope	collapse
η3B	$\eta = 3$, $a/r_e = 0.5$	0.5619	8k	2	none	isothermal

[1] initial distribution corresponding to *run C1* in Taruya & Sakagami (2003c)
[2] initial distribution corresponding to *run C2* in Taruya & Sakagami (2003c)

shows that the trajectory is located around $S_{\rm BG} \simeq 3.7 - 3.9$ and the evolution slows down after contacting with the trajectory of the isothermal distribution. As for the trajectory of the run $\eta 1.5B$, it first goes across the boundary between the stable and the unstable stellar polytropes indicated by the dotted line. Then, it temporarily settles down into a stable stellar polytropic state with index $n \simeq 12 - 14$ for a long time. At that time, the transient states were successfully fitted by the stable stellar polytropic distribution (see Fig.20). It is interesting to note that the growth of the entropy shown in the right panel of Figure 23 is slightly restrained during the quasi-equilibrium regime, which might manifest the minimum entropy production principle in non-equilibrium thermodynamics. On the other hand, for the trajectory of the run $\eta 1C$, while it first approaches the stability boundary, the decreases of the density contrast eventually terminate at relatively higher value $D \simeq 10^4$ and accordingly the transients could not be fitted by the stable stellar polytropes.

Note also that the transient state of the run $\eta 1C$ cannot be even fitted by the *unstable* stellar polytropes, since the density profile of the unstable polytropes shows a log-periodic behavior at the outer part (e.g., Chandrasekhar 1939) while no such behavior appears in the N-body simulation. In this sense, only the quasi-equilibrium state characterized by the *stable* stellar polytropes might have some special meanings. Similar to the isothermal distribution, the quasi-equilibrium state has the quasi-attractive feature that the system starting from some classes of initial conditions tends to approach the polytropic state, which may provide an important suggestion for the reality of the non-extensive statistics.

5 DISCUSSION & CONCLUSION

In this paper, we have discussed a possible application of non-extensive thermostatistics to the stellar systems and attempted to explore its reality. To do this, we have numerically investigated the quasi-equilibrium properties of the N-body systems before the core-collapse stage. Particularly focusing on the long-term stellar dynamical evolution from the thermostatistical

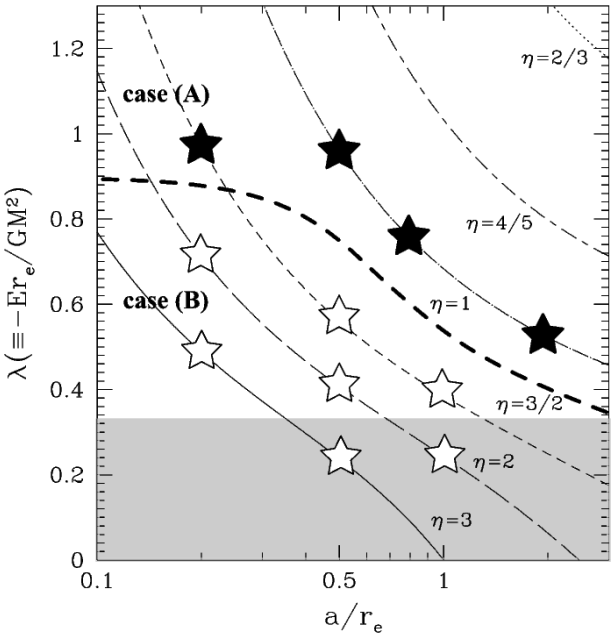

Figure 18. Energy-scale radius relationship in stellar models by Tremaine et al. (1994) in presence of an adiabatic wall. The thin lines represent the equilibrium sequences of stellar model with different values of index η. Along each line, we plot the star symbols, which indicate the result of N-body simulations fitted to the stellar polytropes. The fitting results shown in the figure are categorized as case (A) and case (B), which are roughly separated by thick dashed line. The case (A) denoted by filled symbols means that fitting to the (stable) stellar polytropes was failed, while the case (B) denoted by open symbols indicates that the transient states approximated by the stellar polytropic distribution appeared as quasi-equilibrium state.

point-of-view, we try to characterize the out-of-equilibrium state starting with various initial conditions in the setup of the so-called Antonov problem. We found that the quasi-equilibrium states, in which the system evolves gradually on timescales of two-body relaxation, appears and the system may follow the quasi-equilibrium sequence for a long time if the dimensionless energy $\lambda = -Er_e/GM^2$ of the system is not so far from the critical energy of the isothermal sphere, $\lambda_{\rm crit} = 0.335$. The schematic illustration of our basic results is shown in figure 24. The transient states during the quasi-equilibrium evolution are approximately described by the one-parameter family of stellar polytropes as extremum states of non-extensive entropy S_q with the time-varying polytrope index. The fitted value of the index n gradually increases with time and the system keeps following a sequence of stellar polytropes until reaching the critical index, $n_{\rm crit}$. In general, the condition for the quasi-equilibrium state would depend on the details of the velocity structure in the initial conditions, however, within a class of initial conditions examined in this paper (i.e., stellar polytropes and stellar models with cusped density profiles), the out-of-equilibrium states with inner density profiles $\rho \propto r^{-\alpha}$ ($\alpha < 2$) (or $\eta \leqslant 1$) exhibit the quasi-equilibrium behavior that is attracted to a sequence of stellar polytropes.

One may naively think that the results obtained here severely depend on the presence of an adiabatic wall, since the real stellar systems in absence of the adiabatic wall are known to be poorly fitted to the stellar polytropes. Recalling the discussion in section 4.2.3, however, the outer part of the system is expected to be mainly affected by the boundary condition, since the relaxation timescale at the outer part is rather longer than that at the core. In other words, as long as the relaxation time at the central part is shorter than that at the outer part, the modification of the boundary condition only alters the outer part of the system, not all of the system. In fact, we have seen in section 4.2.3 that the phenomenological King model which accounts for the globular clusters affected by the Galactic tidal field resembles the stellar polytropes at the inner part. In this sense, the stellar polytropic system as quasi-equilibrium state would be a fundamental stellar model and may sometimes make sense even if removing the adiabatic wall (Taruya & Sakagami 2003c).

The present results may give an interesting suggestion for the justification and/or the realization of the non-extensive thermostatistics based on the Tsallis entropy. Strictly speaking, however, the N-body simulations just indicate a reality of the stellar polytropes as *q-analogue* of the Boltzmann-Gibbs distribution. Further, the quasi-equilibrium state is time-dependent, which cannot be rigorously treated by the thermostatistics (Chavanis & Sire 2004). Even at this moment, it might be also possible to give the interpretation that stellar polytrope is merely a dynamical equilibrium state, but it can be stable even with respect to a non-linear perturbation (Chavanis 2003). In this respect, the present N-body results are not conclusive and the interpretation of their results should be carefully discussed. Nevertheless, one may hope that the exploration of a connection with non-extensive entropy opens a new window to understand the non-equilibrium thermodynamics of the long-range systems. In this respect, the analytical treatment based on the kinetic theory is an important next step to interpret the N-body results thermodynamically. A crucial task is to estimate the timescales for quasi-equilibrium evolution, as well as to determine the generic criteria for quasi-equilibria. To investigate this, the Fokker-Planck model for stellar dynamics would

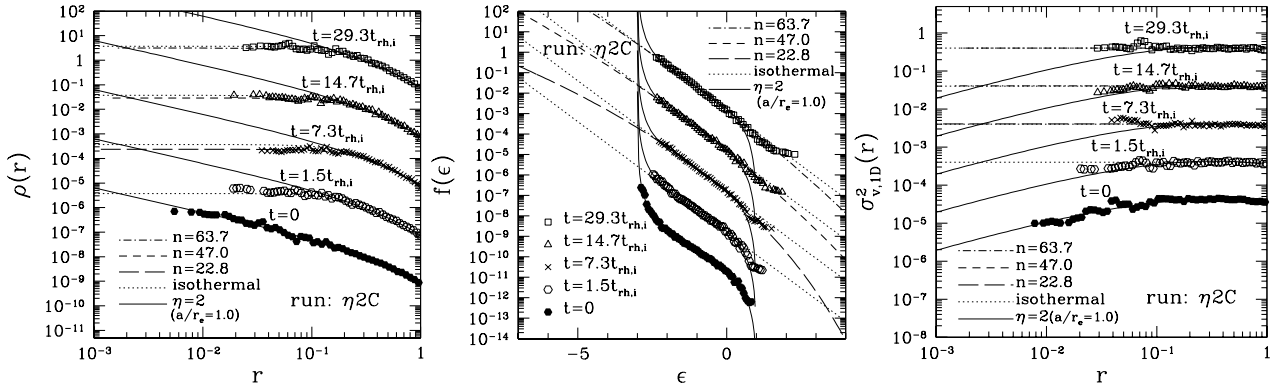

Figure 19. Snapshots of density profile, distribution function and velocity dispersion for run $\eta 2C$.

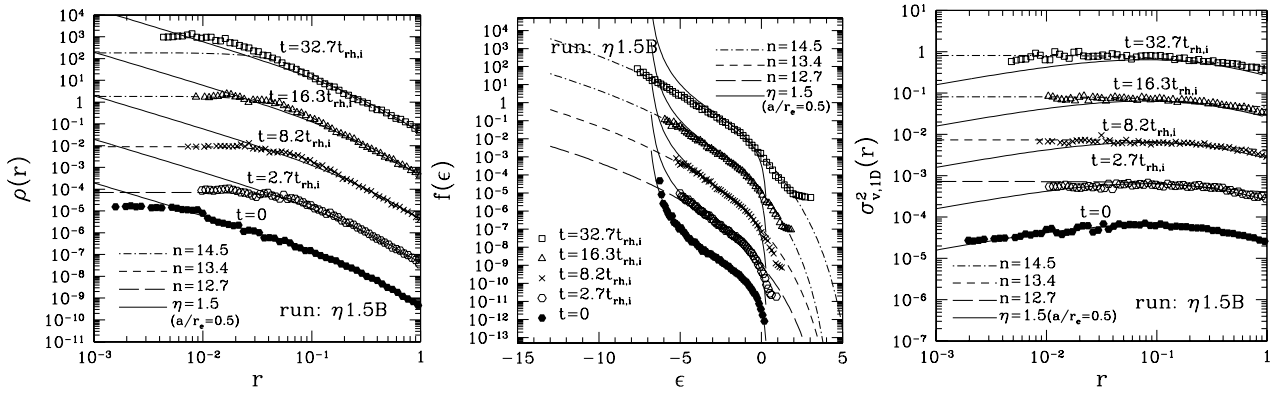

Figure 20. Snapshots of density profile, distribution function and velocity dispersion for run $\eta 1.5B$.

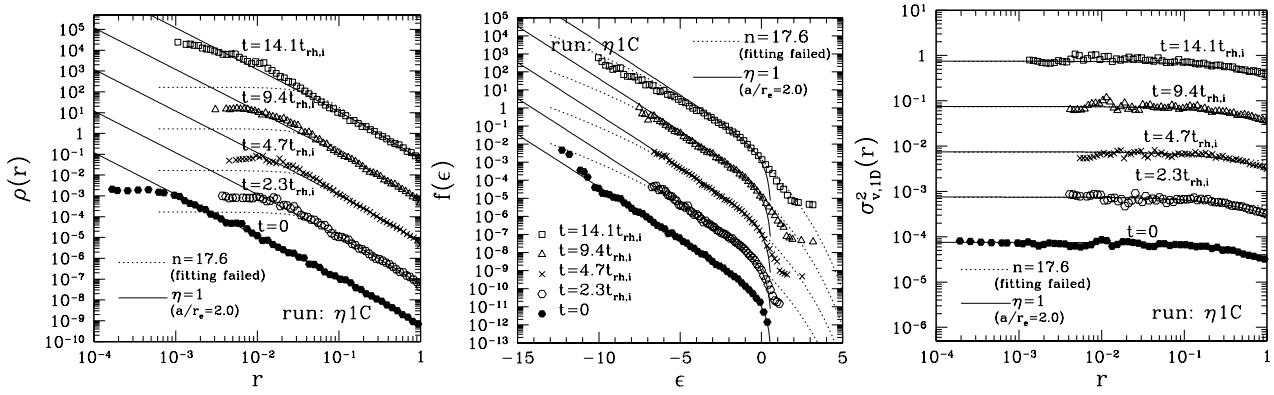

Figure 21. Snapshots of density profile, distribution function and velocity dispersion for run $\eta 1C$.

be helpful Taruya & Sakagami (2004). A quantitative comparison between a numerical solution of the Fokker-Planck model with the N-body results based on a more sophisticated N-body code such as the one developed by Aarseth will be presented elsewhere.

ACKNOWLEDGMENTS

We are grateful to T. Fukushige for providing us the GRAPE-6 code and for his constant supports and helpful comments. We also thank S. Inagaki and K. Takahashi for their comments and suggestions to our future works on the Fokker-Planck model for stellar dynamics. Numerical computations were carried out at ADAC (the Astronomical Data Analysis Center) of the National Astronomical Observatory of Japan. This work was supported by the grand-in-aid for Scientific Research of Japan Society of Promotion of Science (No.14740157, 15540368).

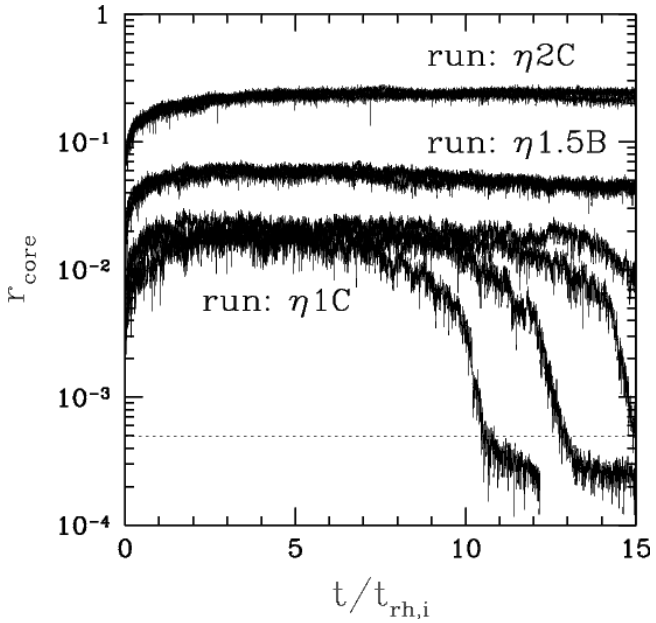

Figure 22. Run-by-Run variation of evolution of core radius among three different realization for the runs $\eta 1.5B$ and $\eta 2C$, and among four different realization for the run $\eta 1C$. The dotted line indicates the length of the potential softening, $\epsilon = 4/N \simeq 4.9 \times 10^{-4}$.

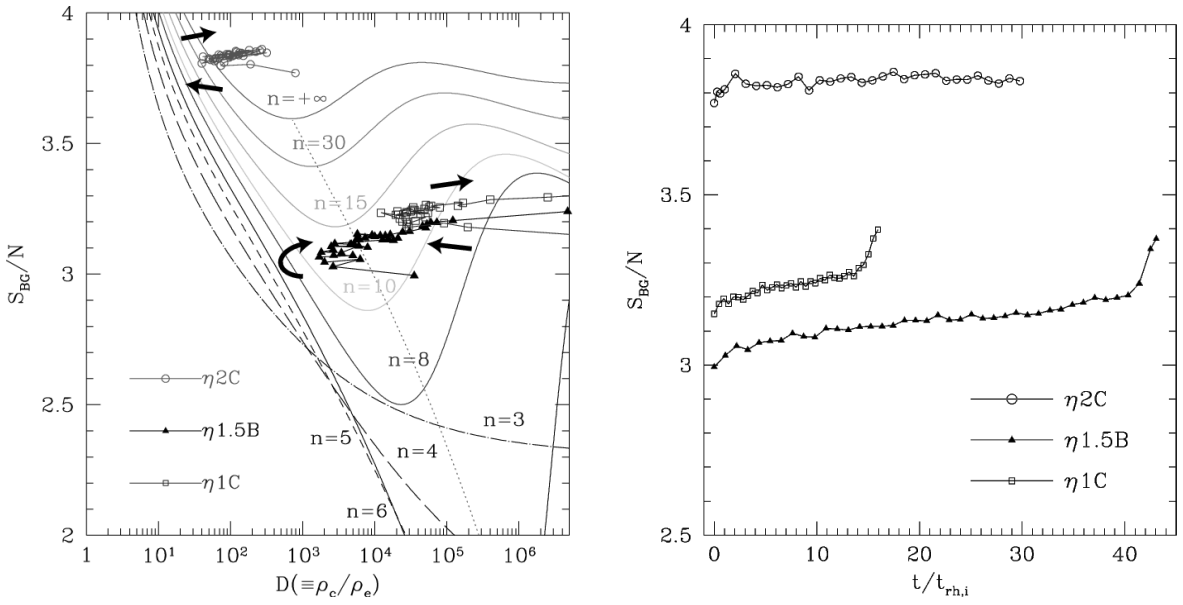

Figure 23. *left*: Trajectories in $(S_{\rm BG}, D)$-plane obtained from the runs $\eta 1C$(*open-squares*), $\eta 1.5B$(*filled triangles*) and $\eta 2C$(*open-circles*). The lines with symbols indicate the simulation results, while the solid, the short-dashed, the long-dashed and the dot-dashed lines are the equilibrium sequences of stellar polytropes with different polytrope index n, which are obtained from the analytic results in Appendix C. On the other hand, the dotted curve represents the stability boundary of the stellar polytropes, inferred from the energy-density contrast relation (dotted curve in Fig.2). *Right*: Time evolution of Boltzmann-Gibbs entropy from the runs $\eta 1C$, $\eta 1.5B$ and $\eta 2C$.

APPENDIX A: CONVERGENCE TEST OF N-BODY SIMULATION

In a series of our N-body simulations, the Plummer softening with parameter $\epsilon = 1/N$ or $4/N$ is used to avoid the formation of tight binaries. For our investigation of the quasi-equilibrium state before the core-collapse stage, the fourth order Hermite integration code with individual time-step provides a robust numerical method without a regularization scheme. However, it would be crucial to pursue the gravothermally unstable regime. While our primary concern is the non-equilibrium evolution before entering the core-collapse phase, it is important to note the effect of potential softening on the estimation of collapse time.

To quantify this, convergence property of the collapse time is investigated by varying the softening parameter ϵ. For this

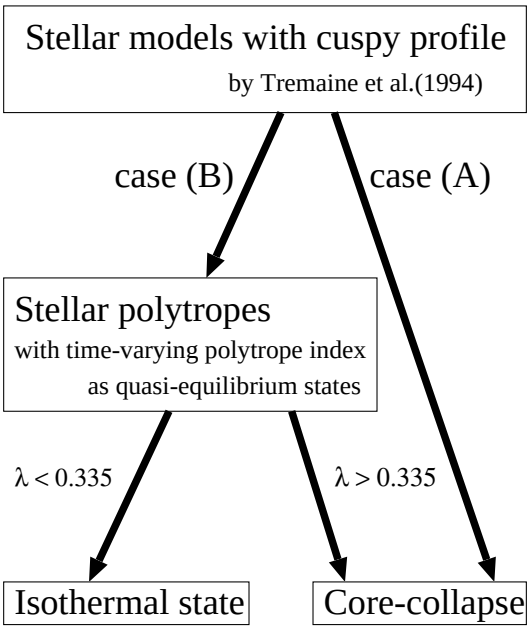

Figure 24. Schematic illustration of the simulation results, which summarizes the evolutionary status shown in figures 2 and 18

purpose, N-body simulations starting with the Plummer model, i.e., the stellar polytrope with index $n = 5$, are used to study the effect of potential softening. The corresponding simulations are the runs $n5B$ and $n5D$ listed in table 2.

Figure 1 shows the results of the convergence test based on the run $n5B$. Left panel plots the evolution of core radii for various choices of softening parameter, while the right panel estimate the collapse time as function of softening parameter ϵ for three different realizations of the initial condition. Here, the collapse time is defined as the first passage time when the core radius becomes shorter than 3ϵ. Clearly, large value of the softening parameter overestimates the estimation of the core-collapse time and the transition between the quasi-equilibrium stage to the core-collapse phase becomes uncertain. For an appropriately small value $\epsilon \lesssim 1/(4N) \simeq 1.2 \times 10^{-4}$, the core radius sharply falls off around the core-collapse time and the collapse time seems to converge to $t_{\rm coll} \sim$ 30-40$t_{\rm rh,i}$, although there exists a large scatter among three different realizations of the initial condition.

In general, the convergence properties of the collapse time depend on the initial conditions. Figure 2 shows the results from the run $n5D$, i.e., Plummer model with density contrast $D = 10^6$. In this case, the scatter becomes even smaller and the collapse time converges to $t_{\rm coll} \sim 18t_{\rm rh,i}$ at $\epsilon \lesssim 6 \times 10^{-5}$, slower than the case of run $n5B$. These experiments indicate that a large softening length affects not only the core-collapse time but also the timescales of quasi-equilibrium stage. Further, the requirement for the softening parameter becomes severe as increasing the initial density contrast. Hence, for quantitative estimation of collapse time, the softening length should be set to zero with implementing a regularization scheme. The use of a small softening length is also favorable to investigate the quasi-equilibrium evolution. Figures 1 and 2 suggest that for initial conditions with moderate range of the initial density contrast, $10^2 \leqslant D \leqslant 10^4$, the softening length with $\epsilon \leqslant 1/N$ provides a better estimation of the quasi-equilibrium timescales, although it still overestimates the collapse time. Hence, in this paper, we mainly use the softening length $\epsilon = 1/N$.

APPENDIX B: A FAMILY OF STELLAR MODEL WITH CUSPS

In this appendix, we present analytic formulae for the stellar model considered by Tremaine et al. (1994) taking account of the adiabatic wall.

Just for convenience, let us first introduce the following variables:

$$A = \eta\, \frac{M}{4\pi a^3}, \qquad B = \frac{GM}{a}\left(\frac{r_e + a}{r_e}\right)^{\eta}. \tag{1}$$

In terms of these, the density profile for stellar models by Tremaine et al. (1994) is expressed as

$$\rho(r) = \frac{A}{(r/a)^{3-\eta}(1 + r/a)^{1+\eta}}. \tag{2}$$

The corresponding mass profile and the gravitational potential respectively becomes

$$m(r) = \int_0^r dr'\; 4\pi\, r'^2\, \rho(r') = \frac{4\pi a^3 A}{\eta}\left(\frac{r}{r+a}\right)^{\eta}, \tag{3}$$

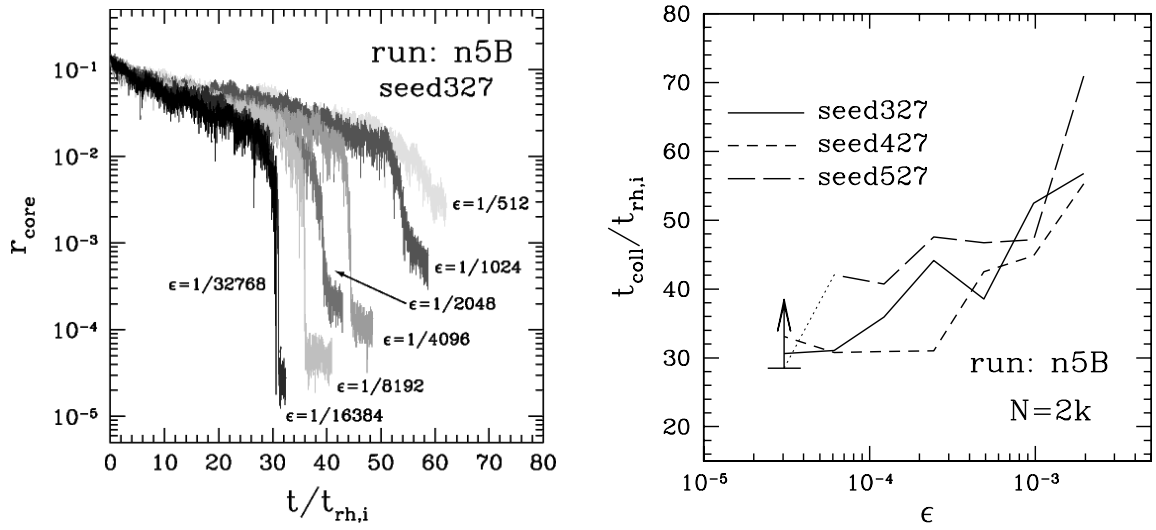

Figure 1. Convergence properties of collapse time for various choices of softening parameter ϵ in the case of run $n5B$. Here, the collapse time is defined as the first passage time when the core radius becomes shorter than 3ϵ. *Left*: evolution of core radius for a realization with seed number 327. *Right*: Variation of collapse time as function of softening parameter among three realizations with different random seed numbers.

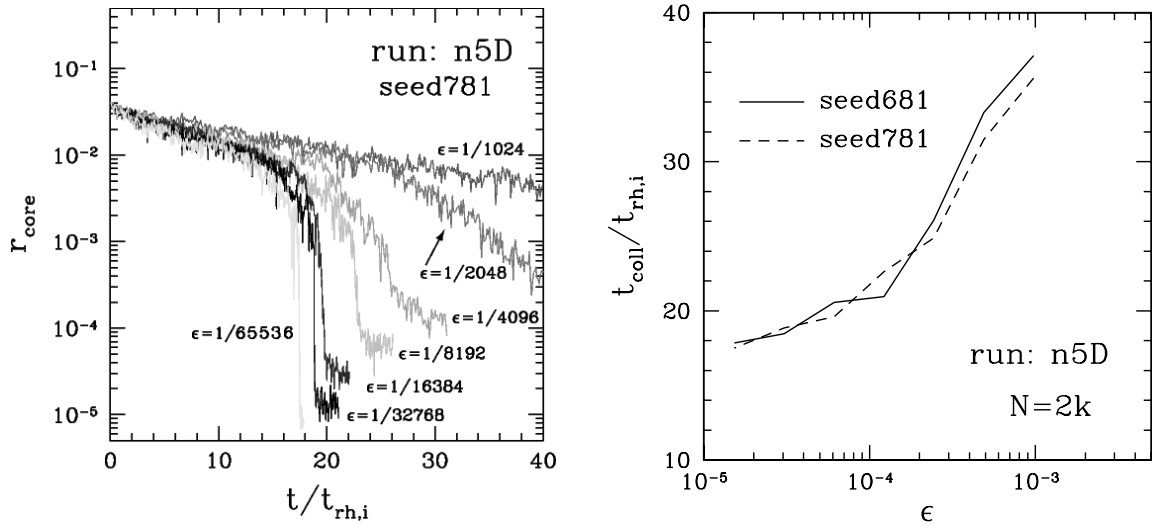

Figure 2. Same as Fig.1, but in the cases of run $n5D$.

and

$$\Phi(r) = -G\left\{\frac{m(r)}{r} + \int_0^{r_e} dr'\ 4\pi r'\rho(r')\right\}$$
$$= \begin{cases} -B\left\{\dfrac{1}{\eta-1}\left(\dfrac{r_e}{r_e+a}\right)^{\eta-1} - \dfrac{1}{\eta-1}\left(\dfrac{r}{r+a}\right)^{\eta-1} + \dfrac{(r_e/a)^{\eta-1}}{(r_e/a+1)^{\eta}}\right\} & ;\quad \eta \neq 1 \\ -B\left\{\log\left(\dfrac{r_e}{r_e+a}\right) - \log\left(\dfrac{r}{r+a}\right) + \dfrac{1}{r_e/a+1}\right\} & ;\quad \eta = 1 \end{cases} \tag{4}$$

For stationary state of the Vlasov equation, the one-dimensional velocity dispersion profile can be calculated from the density profiles and the gravitational potential through the Jeans equation. In the case of the isotropic velocity distribution, this gives

$$\sigma^2_{\mathrm{v,1D}}(r) = \frac{P(r)}{\rho(r)}, \tag{5}$$

with the function $P(r)$ being pressure, determined from the hydrostatic equilibrium(Jeans equation), $dP/dr = -\rho\ d\Phi/dr$.

Note that the explicit expression for function $P(r)$ cannot be expressed in an unified manner. For some values of η, we have

$$P_{\eta=1}(r) = AB\left[6\log\left(\frac{y+1}{y}\right) - \frac{1}{y^2}\left\{6(1+y) - 9 + \frac{2}{y+1} + \frac{1}{2(y+1)^2}\right\}\right], \tag{6}$$

$$P_{\eta=1.5}(r) = AB\left[4\log\left(\frac{y}{y+1}\right) + \frac{1}{y}\left\{4 - \frac{2}{y+1} - \frac{2}{3(y+1)^2} - \frac{1}{3(y+1)^3}\right\}\right], \tag{7}$$

$$P_{\eta=2}(r) = AB\left[4\log\left(\frac{y+1}{y}\right) - \left\{\frac{1}{y+1} + \frac{1}{2(y+1)^2} + \frac{1}{3(y+1)^3} + \frac{1}{4(y+1)^4}\right\}\right], \tag{8}$$

$$P_{\eta=3}(r) = AB\left[\frac{1}{5(y+1)^5} - \frac{1}{6(y+1)^6}\right], \tag{9}$$

where we defined $y = r/a$. Provided the pressure, one can also calculate the total energy of the system confined in a wall as

$$\begin{aligned} E = K + U &= \int d^6 d^3\boldsymbol{x} d^3\boldsymbol{v}\left\{\frac{1}{2}v^2 + \frac{1}{2}\Phi(r)\right\} f(r,v) \\ &= \frac{3}{2}\int_0^{r_e} dr\ 4\pi r^2 P(r) + \frac{1}{2}\int_0^{r_e} dr\ 4\pi r^2 \rho(r)\Phi(r). \end{aligned} \tag{10}$$

In terms of the dimensionless variable $\lambda = -r_e E/(GM^2)$, we obtain

$$\lambda_{\eta=1} = \frac{1}{4}\left(1 + 5y_e + 18y_e^2 + 12y_e^3\right) - 3y_e^2(y_e+1)^2\log\left(\frac{y_e+1}{y_e}\right), \tag{11}$$

$$\lambda_{\eta=1.5} = \frac{1}{8}\left(-3 - 43y_e - 60y_e^2 - 24y_e^3\right) - 3(y_e+1)^3\log\left(\frac{y_e}{y_e+1}\right), \tag{12}$$

$$\lambda_{\eta=2} = \frac{1}{12}\left(29 + 53y_e + 42y_e^2 + 12y_e^3\right) - (y_e+1)^4\log\left(\frac{y_e+1}{y_e}\right), \tag{13}$$

$$\lambda_{\eta=3} = \frac{1}{20y_e^2}\left(1 + 7y_e + y_e^2\right)(y_e - 1), \tag{14}$$

where the variable y_e denotes r_e/a.

According to the standard text book for stellar dynamics, the one-particle distribution function for the isotropic spherical stellar model is expressed as a function of the specific energy $\epsilon = v^2/2 + \Phi(r)$ and can be reconstructed from the density profiles through the Eddington formula. Introducing the variables $\varepsilon = \Phi_0 - \epsilon$ and $\psi = \Phi_0 - \Phi(r)$, we have

$$f(\epsilon) = \frac{1}{\sqrt{8}\pi^2}\int_0^{\varepsilon}\frac{d^2\rho}{d\psi^2}\frac{d\psi}{\sqrt{\varepsilon - \psi}} \tag{15}$$

with the regularity condition:

$$\left(\frac{d\rho}{d\psi}\right)_{\psi=0} = 0. \tag{16}$$

Note that the numerical constant Φ_0 is determined from the above condition. With the use of the analytical expressions (2) and (4), after some manipulation, the Eddington formula (15) can be rewritten with

$$f(\epsilon) = \frac{1}{\sqrt{8}\pi^2}\frac{A}{B^{3/2}}\int_0^{q(\epsilon)}\frac{d\psi}{\sqrt{q(\epsilon) - \psi}}\frac{12\{s(\psi)\}^2 - 4(\eta-4)s(\psi) + 2(3-\eta)}{\{s(\psi)\}^{\eta+1}\{1+s(\psi)\}^{3-\eta}}, \tag{17}$$

where the functions $q(\epsilon)$ and $s(\psi)$ are respectively given by

$$q(\epsilon) = -\frac{\epsilon}{B} - \frac{1}{\eta-1}\left\{\left(\frac{r_e}{r_e+a}\right)^{\eta-1} - 1 + (\eta-1)\frac{(r_e/a)^{\eta-1}}{(r_e/a+1)^{\eta}}\right\}, \tag{18}$$

$$s(\psi) = \frac{\{1-(\eta-1)\psi\}^{1/(\eta-1)}}{1 - \{1-(\eta-1)\psi\}^{1/(\eta-1)}} \tag{19}$$

in cases with $\eta \neq 1$ and

$$q(\epsilon) = -\frac{\epsilon}{B} - \log\left(\frac{r_e}{r_e+a}\right) - \frac{1}{r_e/a+1}, \tag{20}$$

$$s(\psi) = \frac{1}{e^{\psi} - 1} \tag{21}$$

for $\eta = 1$. In principle, the distribution function $f(\epsilon)$ is obtained from the numerical integration of (15). In some specific

values of η, however, one can luckily obtain the analytic expressions of $f(\epsilon)$:

$$f_{\eta=1}(\epsilon) = \frac{A}{B^{3/2}}\sqrt{\frac{2}{\pi^3}}\left[\sqrt{\frac{2}{\pi}}F\left(\sqrt{2q}\right) - \frac{2}{\sqrt{\pi}}F(\sqrt{q}) - e^q\,\mathrm{erf}(\sqrt{q}) + \frac{e^q}{\sqrt{2}}\,\mathrm{erf}\left(\sqrt{2q}\right)\right], \tag{22}$$

$$f_{\eta=1.5}(\epsilon) = \frac{A}{B^{3/2}}\frac{1}{\sqrt{8}\pi^2(2-q)^{9/2}}\left[\frac{3}{2}(3+32q-8q^2)\sin^{-1}\left(\sqrt{\frac{q}{2}}\right)\right.$$
$$\left. -\frac{\sqrt{q(2-q)}}{28}\left\{63+693q-5670q^2+7410q^3-4488q^4+1448q^5-240q^6+16q^7\right\}\right], \tag{23}$$

$$f_{\eta=2}(\epsilon) = \frac{A}{B^{3/2}}\frac{1}{4\sqrt{2}\pi^2}\frac{1}{(1-q)^{5/2}}\left[3\sin^{-1}(\sqrt{q}) - \sqrt{q(1-q)}\,(16q^3-24q^2+2q+3)\right], \tag{24}$$

$$f_{\eta=3}(\epsilon) = \frac{A}{B^{3/2}}\frac{1}{\pi^2(1-2q)}\left[2\sqrt{2q}\,(3-4q) + 3(1-2q)\,\log\left(\frac{1-\sqrt{2q}}{1+\sqrt{2q}}\right)\right]. \tag{25}$$

Here, the function $F(x)$ and $\mathrm{erf}(x)$ are Dawson's integral and the error function:

$$\mathrm{erf}(x) = \sqrt{2}\,\pi\int_0^x dt\; e^{-t^2}, \qquad F(x) = e^{-x^2}\int_0^x dt\; e^{t^2}. \tag{26}$$

Compared the final expressions (22)–(25) with those obtained by Tremaine et al. (1994), we deduce that the only alternation in the expressions of Tremaine et al. (1994) in presence of the adiabatic boundary is to replace all the variables ϵ at the right-hand side of equations with the function $q(\epsilon)$ defined above. Therefore, the above results consistently recover the formulas derived by Tremaine et al. (1994) in the limit $r_e \to \infty$.

APPENDIX C: BOLTZMANN-GIBBS ENTROPY FOR STELLAR POLYTROPES

Here, we derive the explicit expression for Boltzmann-Gibbs entropy in the case of the stellar polytropic distribution, which is shown in theoretical curves of figure 23.

First, we substitute the stellar polytropic distribution (12) into the definition of Boltzmann-Gibbs entropy:

$$S_{\mathrm{BG}}^{(\mathrm{poly})}/N = -\int d^3\boldsymbol{x}d^3\boldsymbol{v}\,\left(\frac{f^{(\mathrm{poly})}}{N}\right)\ln\left(\frac{f^{(\mathrm{poly})}}{N}\right)$$
$$= -(s_A+s_B+s_C). \tag{27}$$

The quantities s_A, s_B and s_C involving the phase-space integral are separately evaluated as

$$s_A = \frac{1}{4\sqrt{2}\pi\;B(3/2,n-1/2)}\,\ln\left\{\frac{1}{4\sqrt{2}\pi\,B(3/2,n-1/2)}\right\}\int d^3\boldsymbol{x}d^3\boldsymbol{v}\;\frac{\rho/M}{\{(n+1)P/\rho\}^{3/2}}\left\{1-\frac{v^2/2}{(n+1)P/\rho}\right\}^{n-3/2}$$
$$= \ln\left\{\frac{1}{4\sqrt{2}\pi\,B(3/2,n-1/2)}\right\}, \tag{28}$$

$$s_B = \frac{1}{4\sqrt{2}\pi\;B(3/2,n-1/2)}\int d^3\boldsymbol{x}d^3\boldsymbol{v}\,\frac{\rho/M}{\{(n+1)P/\rho\}^{3/2}}\left\{1-\frac{v^2/2}{(n+1)P/\rho}\right\}^{n-3/2}\ln\left\{1-\frac{v^2/2}{(n+1)P/\rho}\right\}^{n-3/2}$$
$$= \left(n-\frac{3}{2}\right)\{\psi(n-1/2)-\psi(n+1)\}\int d^3\boldsymbol{x}\frac{\rho}{M}$$
$$= \left(n-\frac{3}{2}\right)\{\psi(n-1/2)-\psi(n+1)\}, \tag{29}$$

$$s_C = \frac{1}{4\sqrt{2}\pi\;B(3/2,n-1/2)}\int d^3\boldsymbol{x}d^3\boldsymbol{v},\,\frac{\rho/M}{\{(n+1)P/\rho\}^{3/2}}\left\{1-\frac{v^2/2}{(n+1)P/\rho}\right\}^{n-3/2}\ln\frac{\rho/M}{\{(n+1)P/\rho\}^{3/2}}$$
$$= \int d^3\boldsymbol{x}\frac{\rho}{M}\,\ln\frac{\rho/M}{\{(n+1)P/\rho\}^{3/2}}. \tag{30}$$

Here, the functions $\psi(z)$ and $B(a,b)$ are the digamma and the beta functions, respectively. Collecting the above terms, the Boltzmann-Gibbs entropy becomes

$$S_{\mathrm{BG}}^{(\mathrm{poly})}/N = \ln\{4\sqrt{2}\,\pi\;B\left(\frac{3}{2},n-\frac{1}{2}\right)\} - \left(n-\frac{3}{2}\right)\left\{\psi\left(n-\frac{1}{2}\right)-\psi\,(n+1)\right\} - \int d^3\boldsymbol{x}\,\frac{\rho}{M}\,\ln\left\{\frac{\rho/M}{\{(n+1)P/\rho\}^{3/2}}\right\}.$$

For the remaining integral in the above expression, a further reduction is possible by repeating the integration by part.

Using the equations of hydrostatic equilibrium, a straightforward calculation yields

$$\int d^3\boldsymbol{x}\,\frac{\rho}{M}\,\ln\frac{\rho/M}{\{(n+1)P/\rho\}^{3/2}} = -\ln M\left\{\frac{(n+1)P_e}{\rho_e^{1+1/n}}\right\}^{3/2} + \\ +\frac{n-3/2}{n}\left[\ln\rho_e - \frac{n}{n+1}\frac{GM\rho_e}{P_e r_e} - \frac{8\pi r_e^3\rho_e}{M} + 6 + \frac{n}{(n+1)^2}\int_0^{r_e} dr\left(\frac{\rho}{P}\right)^2\frac{G^2m^3}{Mr^3}\right]. \quad (31)$$

Note that the subscript $_e$ denotes the quantities evaluated at the wall, $r = r_e$. In terms of the homology invariants (u, v) defined in equations (21) and (22), the entropy $S_{\rm BG}$ is finally expressed as:

$$S_{\rm BG}^{(\rm poly)}/N = -6\left(\frac{n-3/2}{n}\right) - \left(n-\frac{3}{2}\right)\left\{\psi\left(n-\frac{1}{2}\right) - \psi\left(n+1\right)\right\} \\ + \left(\frac{n-3/2}{n+1}\right)v_e + 2\left(\frac{n-3/2}{n}\right)u_e - \ln\left(\frac{u_e v_e^{3/2}}{4\pi}\right) + \frac{3}{2}\ln(2\pi GMr_e) \\ + \ln\left\{2\pi(n+1)^{3/2}\,B\left(\frac{3}{2}, n-\frac{1}{2}\right)\right\} - \frac{n-3/2}{(n+1)^2}\int_0^{r_e} dr\left(\frac{\rho}{P}\right)^2\frac{G^2m^3}{Mr^3}. \quad (32)$$

In the limit $n \to \infty$, we correctly recover the Boltzmann-Gibbs entropy for the isothermal state:

$$S_{\rm BG}^{(\rm iso)}/N = -\frac{9}{2} + v_e + 2u_e - \ln\left(\frac{u_e v_e^{3/2}}{4\pi}\right) + \frac{3}{2}\ln(2\pi GMr_e). \quad (33)$$

REFERENCES

Aarseth S.J., Hénon, M., Wielen, R., 1974, A&A 37, 183
Aarseth S.J., 2003, *Gravitational N-body Simulations*, Cambridge Univ. Press, Cambridge, UK
Abe S., Okamoto Y., 2001, *Non-extensive Statistical Mechanics and Its Applications*, Springer, Berlin
Antonov V.A., 1962, Vest. Leningrad Gros. Univ. 7, 135
Baumgardt H., Makino J., 2003, MNRAS 340, 227
Binney J., Merrifield M., 1998, *Galactic Astronomy*, Princeton Univ. Press, Princeton, NJ
Binney J., Tremaine S., 1987, *Galactic Dynamics*, Princeton Univ. Press, Princeton, NJ
Bettwieser E., Sugimoto D., 1984, MNRAS 208, 493
Casertano S., Hut P., 1985, ApJ 298, 80
Chandrasekhar S., 1939, *Introduction to the Study of Stellar Structure*, Dover, New York.
Chandrasekhar S., 1943, *Principles of Stellar Dynamics*, Dover Publ.
Chavanis P. H., 2003, A&A 401, 15
Chavanis P. H., Sire C., 2004, Physica A, in press (cond-mat/0409569)
Endoh H., Fukushige T., Makino J., 1997 PASJ 49, 345
Fukushige T., Heggie D. C., 1995, MNRAS 276, 206
Giersz M., Heggie D. C., 1994, MNRAS 268, 257
Heggie, D.C., Hut, P., 2003, *The Gravitational Million-body Problem*, Cambridge Univ. Press, Cambridge, UK
Hernquist L., 1990, ApJ 356, 359
Hut P., Makino J., 1999, Science 283, 501
Jaffe W., 1983, MNRAS 202, 995
Katz J., 1978, MNRAS 183, 765
Katz J., 1979, MNRAS 189, 817
King I.R., 1966, AJ 71, 64
Kippenhahn R., Weigert A., 1990, *Stellar Structure and Evolution*, Springer, Berlin
Lynden-Bell D., Wood R., 1968, MNRAS 138, 495
Makino J., 1996, ApJ 471, 796
Makino J., Fukushige T., Koga M., Namura K., 2003, PASJ 55, 1163
Martínez S., Nicolás F., Pennini F., Plastino A., 2000, Physica A 286, 489
Meylan, G., Heggie, D.C., 1997, A&AR 8, 1
Padmanabhan T., 1989, ApJ Suppl. 71, 651
Padmanabhan T., 1990, Phys.Rep. 188, 285
Plastino A.R., Plastino A., 1993, Phys. Lett. A 174, 384
Quinlan G.D., 1996, New Astron 1, 255
Sakagami M., Taruya A., 2004, Continuum.Mech.Thermodyn. 16, 279 (cond-mat/0310082)
Spitzer L., 1987, *Dynamical Evolution of Globular Clusters*, Princeton Univ. Press, Princeton, NJ
Sugimoto D., Bettwieser, E., 1983, MNRAS 204, 19p
Sugimoto D., Chikada Y., Makino J., Ito T., Ebisuzaki T., Umemura M., 1990, Nature 345, 33

Tanikawa, A., Fukushige, T., 2005, PASJ 57, 155
Taruya A., Sakagami M., 2002, Physica A 307, 185
Taruya A., Sakagami M., 2003a, Physica A 318, 387
Taruya A., Sakagami M., 2003b, Physica A 322, 285
Taruya A., Sakagami M., 2003c, Phys.Rev.Lett. 90, 181101
Taruya A., Sakagami M., 2004, Physica A 340, 453
Trager S.C., King I.R., Djorgovski S., 1995, AJ 109, 218
Tremaine S., Richstone D.O., Byun Y-I., Dressler A., Faber S.M., Grillmair C., Kormendy J., Lauer T.R., 1994, AJ 107, 634
Tsallis C., 1988, J. Stat. Phys. 52, 479
Tsallis C., 1999, Braz. J. Phys. 29, 1
Tsallis C., Mendes R.S., Plastino A.R., 1998, Physica A 261, 534